Palaeogeography, Palaeoclimatology, Palaeoecology 311 (2011) 111–125

Contents lists available at SciVerse ScienceDirect

Palaeogeography, Palaeoclimatology, Palaeoecology

journal homepage: www.elsevier.com/locate/palaeo

Late Jurassic paleoclimate of Central Africa

Timothy S. Myers *, Neil J. Tabor, Louis L. Jacobs

Roy M. Huffington Department of Earth Sciences, Southern Methodist University, Dallas, TX 75275, United States

ARTICLE INFO

Article history:
Received 22 September 2010
Received in revised form 27 July 2011
Accepted 26 August 2011
Available online 3 September 2011

Keywords:
Congo Basin
Stanleyville Group
Paleosols
Paleoclimate
Stable isotopes

ABSTRACT

Paleopedology and geochemical analysis of Upper Jurassic deposits in the Stanleyville Group of Central Africa indicate harsh Late Jurassic paleoclimates in the interior of Gondwana. Subsurface samples collected from the Samba borehole near the center of the Congo Basin show only weak morphological evidence of pedogenesis, but are characterized by an abundance of shrink-swell (vertic) features and rare calcium carbonate nodules, indicating seasonal variations in moisture availability and net soil moisture deficiency, respectively. X-ray diffraction analysis of paleosol matrix material reveals the presence of analcime and the clay mineral palygorskite, strong indicators of hot, arid climatic conditions. The $\delta^{18}O$ and δD values of clay minerals from paleosol profiles range from +22.3‰ to +25.4‰ and −44.4‰ to −39.6‰ SMOW, respectively, and correspond to crystallization temperatures between 25 °C and 40 °C. These crystallization temperatures compare favorably with austral summer surface temperature estimates for Central Africa that result from Late Jurassic global circulation models. Calculations of soil CO_2 production using the $\delta^{13}C$ values of pedogenic carbonates and plant-derived organic matter produce lower CO_2 production estimates for the Stanleyville Group relative to the roughly contemporary Morrison Formation of the western U.S. These low soil CO_2 production estimates provide further support for arid Late Jurassic climate conditions in the Congo Basin. The paleoclimatic conditions inferred here from the Stanleyville Group are similar to those reconstructed from other Upper Jurassic African continental localities between 5°S and 20°S paleolatitude. However, penecontemporaneous terrestrial coastal sites within this latitudinal belt of Gondwana retain evidence of generally wetter conditions, suggesting that those regions may have received more rainfall than the continental interior. The paleoclimatic setting reconstructed here from geologic indicators and geochemical proxies suggests that general circulation models accurately predict unique paleoenvironmental conditions that lack modern analogs.

1. Introduction

The latter half of the Jurassic Period was a time of significant paleogeographic change as fragmentation of Pangea progressed and the incipient North Atlantic developed between North America and Eurasia (Uchupi, 1988; Smith et al., 1994; Golonka et al., 1996). These tectonic rearrangements brought about major changes in both climate and sea level (Parrish, 1993; Hallam, 2001). Global datasets of paleoclimate indicators suggest that low-latitude Late Jurassic environments were arid and tropical ever-wet conditions were absent (Rees et al., 2000). During the Late Jurassic, the African portion of Gondwana straddled the equator (Smith et al., 1994), providing a large area for development of low-latitude continental environments. Some of the Late Jurassic terrestrial ecosystems that developed in eastern Africa boasted diverse faunas that rivaled those of contemporary Europe and North America (Goodwin et al., 1999; Aberhan et al., 2002), but data from this time period are lacking for much of the rest of the continent.

Despite the fact that several east African localities have provided a wealth of vertebrate fossil material (Raath and McIntosh, 1987; Goodwin et al., 1999; Aberhan et al., 2002), Upper Jurassic continental deposits compose only a small portion of the present surficial geology of Africa, and little effort has been devoted to the study of paleoclimatic data recorded in these rocks. Paleoclimate interpretations made from African Upper Jurassic strata are typically restricted to general comments on the presence of climatically-sensitive sedimentary indicators, presented as background information in studies of vertebrate faunas and depositional environments (e.g., Assefa, 1991; Aberhan et al., 2002). Even less is known about the terrestrial environments that developed in the interior of the African continent. The Upper Jurassic–Lower Cretaceous Stanleyville Group of the Congo Basin presents a unique opportunity to study the paleoclimatic conditions of low-latitude, Late Jurassic terrestrial environments deep in the interior of Gondwana.

This study evaluates paleoclimatic conditions during deposition of the Stanleyville Group using paleopedological, mineralogical, and geochemical data. Examination of climatically-sensitive paleosol features and mineralogical composition yields information about relative amounts of precipitation and patterns of annual rainfall distribution, while stable isotope analysis of clay minerals provides

* Corresponding author. Tel.: +1 214 768 1751; fax: +1 214 768 2701.
E-mail address: smyers@smu.edu (T.S. Myers).

0031-0182/$ – see front matter © 2011 Elsevier B.V. All rights reserved.
doi:10.1016/j.palaeo.2011.08.013

quantitative estimates of soil temperature. Soil CO_2 production estimates based on $\delta^{13}C$ values of paleosol calcite and organic matter from both the Stanleyville Group and the Morrison Formation of the western U.S. are compared in order to illustrate potential differences in environmental parameters. Results of this work are also compared with paleogeographic studies of sedimentological and paleobotanical climate indicators and general circulation model (GCM) results for Late Jurassic paleoclimate in low-latitude Africa.

2. Geological background

2.1. Tectonic and paleogeographic setting

During the Late Jurassic, the breakup of Pangea was well underway, but Gondwana remained largely intact, stretching from near the South Pole to ~25°N (Smith et al., 1994; Golonka et al., 1996). The Congo Basin, a large downwarped area atop the Congo craton (Bumby and Guiraud, 2005; Giresse, 2005; Kadima et al., 2011a, 2011b), occupied a position between 10°S and 20°S in the interior of Gondwana (Smith et al., 1994). Formation of the Congo Basin was initiated in the Late Proterozoic (Lawrence and Mvumbi, 1988; Chorowicz et al., 1990), perhaps as the result of failed rifting (Daly et al., 1992; Crosby et al., 2010; Kadima et al, 2011b), and was completed by Early Paleozoic thermal subsidence (Lawrence and Mvumbi, 1988; Daly et al., 1992) that generated accommodation space for Upper Jurassic–Lower Cretaceous strata of the Stanleyville Group.

Within the Congo Basin, the Cuvette Centrale sub-basin, bounded by Precambrian thrust belts, covers an area approximately 1.2 million km^2 and contains up to 9 km of sedimentary fill, ranging in age from Early Cambrian to Recent (Daly et al., 1992; Kadima et al., 2011b). The structural framework of the Cuvette Centrale is dominated by NE–SW trending transfer faults and ESE–WNW trending normal faults formed in the initial Late Proterozoic extensional event (Chorowicz et al., 1990; Kadima et al., 2011b). These faults were later reactivated by Late Cambrian and Permo-Triassic compressional events related to the assembly of Gondwana and Pangea, respectively (Daly et al., 1992; Bumby and Guiraud, 2005; Giresse, 2005; Kadima et al., 2011b). Further reactivation and uplift in the Middle Jurassic was followed by subsidence in the Late Jurassic (Chorowicz et al., 1990; Daly et al., 1992).

In the 1950s, two boreholes were drilled by the Syndicate pour l'Etude Géologique et Minière de la Cuvette Congolaise at Samba and Dekese in order to constrain subsurface stratigraphic architecture for a study of reservoir potential in the Cuvette Centrale (Lawrence and Mvumbi, 1988). The Samba well, the source of the Stanleyville Group samples used in this study, was located near the center of the Congo Basin and penetrated approximately 1170 m of Paleozoic, Mesozoic, and Cenozoic deposits resting atop Precambrian basement (Giresse, 2005; Kadima et al., 2011a). The 6.7 cm diameter cores recovered from the Samba and Dekese boreholes are currently housed in the Royal Museum for Central Africa in Tervuren, Belgium.

2.2. Stratigraphy

The Stanleyville Group (Veatch, 1935), alternatively referred to as the Stanleyville Formation (Daly et al., 1992), crops out along the banks of the Lualaba and Congo rivers in the eastern part of the Cuvette Centrale (Lepersonne, 1974; Cahen, 1983) (Fig. 1A). Boreholes indicate that the Stanleyville Group is also present in the subsurface in the central and far western portions of the basin (Cahen et al., 1959; Egoroff and Lombard, 1962; Cahen, 1983). Eastern outcrop sections are 460 m thick in the type-area near Kisangani (formerly Stanleyville) (Colin, 1994) and consist primarily of reddish-brown and greenish-gray mudstones with interspersed limestones and bituminous beds (Bose, 1974). Subsurface sections to the west, near the basin center at Samba, are dominated by red sandstones and reach a thickness of 323 m (Cahen et al., 1959; Bose, 1974; Cahen, 1983). Boreholes in the far western part of the basin near Kinshasa and Brazzaville contain a mix of red mudstones and sandstones, with a reduced total thickness not greater than 20 m (Egoroff and Lombard, 1962; Bose, 1974; Cahen, 1983). In the Samba core, the Stanleyville Group lies unconformably beneath sandstones of the Lower Cretaceous Loia Group and rests unconformably atop Lower to Middle Paleozoic sandstones correlative with the Aruwimi Group (Kadima et al., 2011a).

2.3. Age and depositional setting

The Stanleyville Group was initially considered to be Upper Triassic in age based on preliminary analysis of fishes collected from eastern outcrops (Leriche, 1911; Veatch, 1935). Subsequent biostratigraphic studies, including more extensive analyses of the Stanleyville fishes (Saint-Seine et al., 1952; Cahen and Lepersonne, 1955; Saint-Seine, 1955; Saint-Seine and Casier, 1962), and additional analyses of ostracodes (Grekoff, 1957), conchostracans (Defrétin-Lefranc, 1967), and bivalves (Cox, 1953, 1960), all support assignment to the Upper Jurassic. Further refinement of the biostratigraphy suggests that the Stanleyville Group extends from the lower Kimmeridgian to the Barremian or Aptian (Lepersonne, 1977; Cahen, 1983). In contrast, Kadima et al. (2011a) cite a palynological report by Stough (1965) that assigns a Middle to Upper Jurassic (Bajocian–Oxfordian) age to the Stanleyville Group. Most recently, Colin (1994) reinterpreted the biostratigraphic evidence in favor of a Middle Jurassic (Aalenian–Bathonian) age, based largely on aspects of the fish and ostracode assemblages. In the past decade, an entirely Middle Jurassic age has been adopted by some (Arratia et al., 2002; López-Arbarello et al., 2008; Rauhut and López-Arbarello, 2009), but not all (Yanbin et al., 2004; Giresse, 2005; Kadima et al., 2011a) researchers. The ostracode assemblage from the Stanleyville Group (Colin, 1994) does not resemble those of the Upper Jurassic Morrison (U.S.A.) or Tendaguru (Tanzania) formations (Schudack et al., 1998; Sames, 2008), but the conchostracan fauna is similar to that of the Upper Jurassic Tacuarembó Formation of Uruguay (Yanbin et al., 2004). Although more detailed work is needed to resolve the questions surrounding the precise age of the Stanleyville Group, this study adheres to the stratigraphic age assignment presented by Cahen (1983).

Biostratigraphic correlation of the subsurface Stanleyville section at Samba with outcrops in the type area near Kisangani indicates that the Jurassic–Cretaceous boundary likely occurs between 1009.26 m and 941.87 m depth in the Samba core (Cahen, 1983). Deposition of the Jurassic portion of the Stanleyville Group was roughly coeval with that of the Morrison Formation of the western U.S., the informally-named Lourinhã formation of western Portugal, and the Tendaguru Formation of Tanzania (Fig. 2; Sames, 2008).

In the Samba core, the Stanleyville Group consists of fluvial and lacustrine deposits (Cahen, 1983; Kadima et al., 2011a). The temporally equivalent fluvio-lacustrine deposits of the Morrison Formation (Kimmerdgian–Tithonian) crop out over a large part of the western U.S., extending from New Mexico northward to Montana, and from Utah eastward to Oklahoma (Kowallis et al., 1998; Foster, 2003; Turner and Peterson, 2004), corresponding to paleolatitudes between 30°N and 35°N (Smith et al., 1994). Morrison Formation samples used here were collected from outcrops near Ghost Ranch, New Mexico; Shell, Wyoming; and Bridger, Montana (Fig. 1B), providing a geographically broad sampling of Morrison environments.

3. Methods

3.1. Field sampling and laboratory analysis

The Stanleyville paleosol samples used in this study come from the Samba core between 1167.43 m and 844.65 m depth. Samples were collected from all parts of this interval that showed evidence

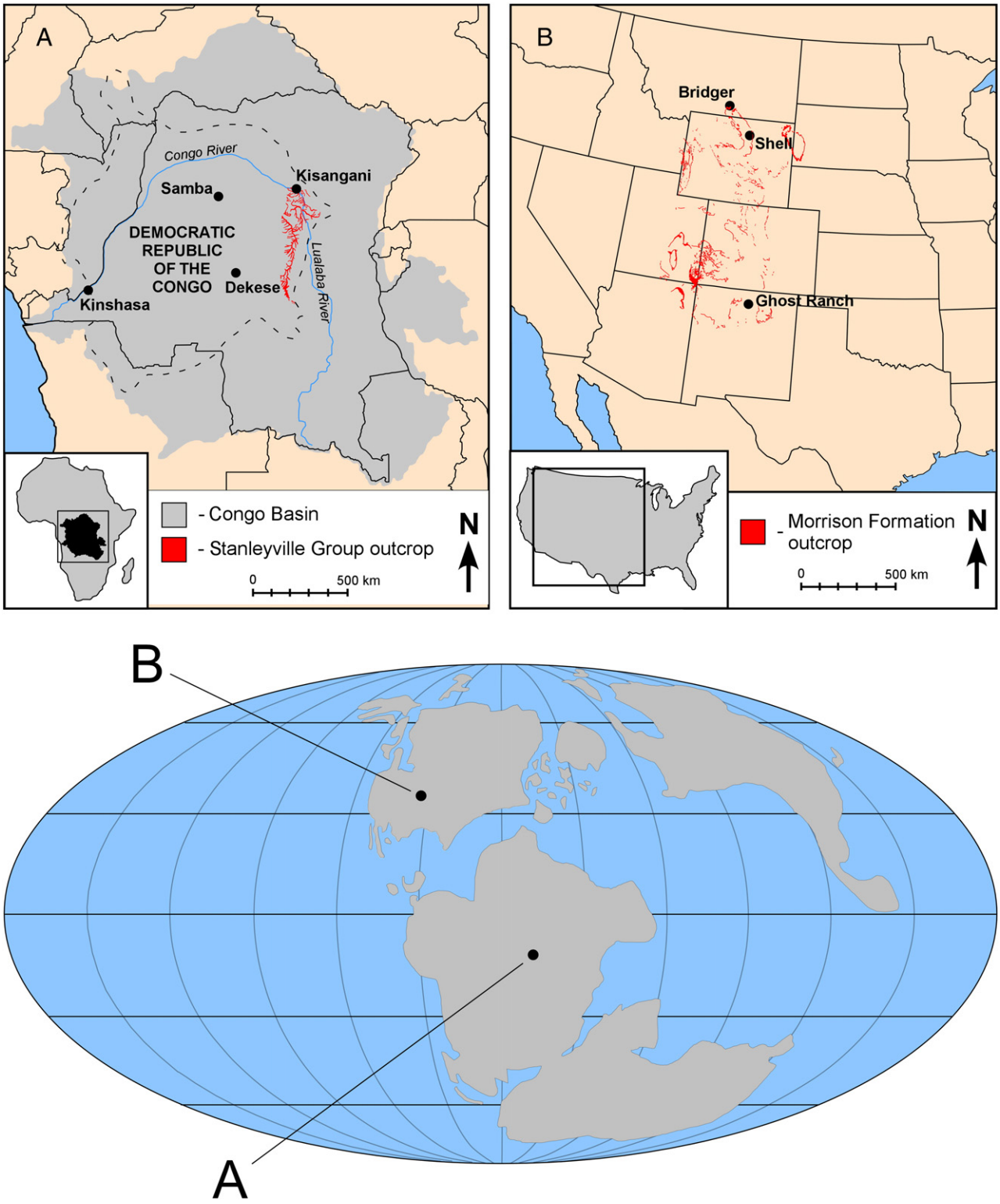

Fig. 1. Maps of the study areas and localities from which samples were collected. Each study area is plotted on the Late Jurassic paleogeographic map below, modified from Smith et al. (1994). (A) Map of Central Africa showing locations mentioned in text and outcrop distribution of the Stanleyville Group based on Lepersonne (1974). The shaded area represents the Congo Basin, and the dashed line denotes the approximate border of the Cuvette Centrale sub-basin. (B) Map of sampling localities and outcrop distribution of the Morrison Formation based on Foster (2003).

of pedogenic modification. Each sample was described in detail, including observations of lithology, Munsell color, sedimentary or pedogenic features, and reactivity with hydrochloric acid. A total of 16 paleosol profiles were identified in the Stanleyville section of the core (Fig. 3), and each profile was classified according to the system developed by Mack et al. (1993).

Stanleyville paleosol samples selected for X-ray diffraction (XRD) analysis were disaggregated in deionized water using an ultrasonic water bath and centrifuged to separate the total clay fraction (<2 μm) from the coarse fraction (>2 μm). The >2 μm size fraction of each sample was powdered with a mortar and pestle and analyzed at SMU using a Rigaku Ultima III X-ray diffractometer with a step size

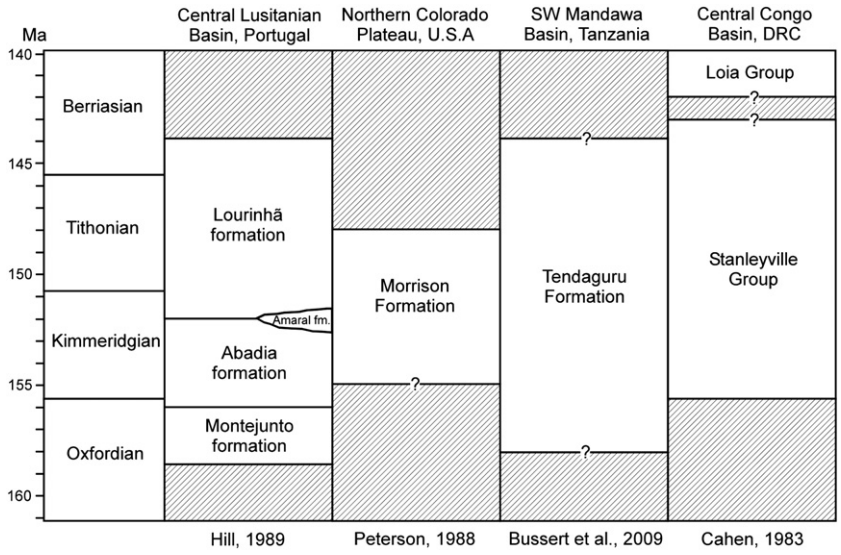

Fig. 2. Correlation chart for Upper Jurassic terrestrial successions of North America, Western Europe, Eastern Africa, and Central Africa. Stratigraphic nomenclature is based on references given at the bottom of each column (Cahen, 1983; Peterson, 1988; Hill, 1989). Depicted ages of the Lourinhã formation, the Tendaguru Formation, and the Stanleyville Group are based on biostratigraphy (Cahen, 1983; Hill, 1989; Sames, 2008). The age of the Morrison Formation is based on radiometric dating (Kowallis et al., 1998).

of 0.05° over a range of 2°–70° 2θ. Using the total clay fraction, oriented aggregates were prepared and mounted on glass slides. Each clay sample was treated to produce (1) K^+-saturated, (2) Mg^{2+}-saturated, and (3) Mg^{2+}-saturated as well as glycerol-solvated mounts. After initial XRD analysis, K^+-saturated samples were heated in a furnace at 500 °C for a minimum of 2 h, and then reanalyzed. Analysis of the total clay fraction was followed by isolation and analysis of the fine clay fraction (<0.2 μm), which contains predominantly pedogenic, rather than detrital, clays in paleosol profiles (Tabor et al., 2002; Vitali et al., 2002). All clay samples were analyzed at SMU using a Rigaku Ultima III X-ray diffractometer with a step size of 0.05° over a range of 2°–30° 2θ. The relative abundance of different clay mineral species in all size fractions was estimated using the area of the 001 peak in the glycerol-solvated mount with background removed.

Four paleosol matrix samples were selected for determination of $\delta^{18}O$ and δD values of phyllosilicates in the fine clay fraction. These samples were treated with a citrate–bicarbonate–dithionite solution to remove iron oxides, then thoroughly rinsed with deionized water at least five times and subsequently dried. Each sample was divided into two aliquots: one for δD analysis and one for $\delta^{18}O$ analysis. The sample fractions selected for δD analysis were dehydrated at ~250 °C for 0.5 to 0.75 h under vacuum to remove any adsorbed or interlayer water. Samples were then heated in 0.16 bar O_2 under closed-system conditions at ~850 °C for 30 min, and water vapor produced by dehydroxylation of the clay minerals was passed over reduced uranium metal at ~760 °C to produce hydrogen gas. H_2 yields were determined by mercury manometry with a precision of ±1 μmol. The isotopic composition of the hydrogen gas was measured at SMU using a Finigan MAT 252 isotope ratio mass spectrometer. Sample fractions reserved for $\delta^{18}O$ analysis were dehydrated in nickel-rod bombs under open-system vacuum at 150 °C for 1 h to remove sorbed water and reacted with bromine pentafluoride to produce oxygen gas (Savin and Epstein, 1970). The O_2 was then reacted with graphite to produce CO_2, which was cryogenically isolated and analyzed for $\delta^{18}O$ values using a Finigan MAT 252 isotope ratio mass spectrometer at SMU. Both δD and $\delta^{18}O$ values are reported in per mil (‰) units relative to Standard Mean Ocean Water (SMOW).

Carbonates in the Samba core were collected and drilled from handsample. Visual inspection revealed no coarsely crystalline, sparry fabrics that typically represent groundwater or diagenetic cements (Mora et al., 1993; Quast et al., 2006). Sample powders were reacted with 100% orthophosphoric acid at 25 °C and cryogenically purified to produce CO_2 (McCrea, 1950). The carbon isotope composition of the extracted CO_2 was measured at SMU using a Finigan MAT 252 isotope ratio mass spectrometer.

Organic matter collected from both the Stanleyville Group and the Morrison Formation consisted of carbonized vascular plant material. All organic samples were treated with dilute HCl to remove any carbonate material, then thoroughly rinsed with deionized water and air-dried. Procedures for combustion of organics to produce CO_2 were based on methods detailed by Boutton (1991). Each sample was sealed under vacuum in a vycor combustion tube with ~1 g copper oxide and 0.5 g native copper, then pyrolized in a muffle furnace. Samples were heated at 900 °C for 2 h, then the furnace temperature was incrementally reduced and held at 650 °C for 2 h. Carbon dioxide evolved during pyrolization was extracted and analyzed at SMU using a Finigan MAT 252 isotope ratio mass spectrometer. Carbon isotope composition is reported here in per mil (‰) relative to the PeeDee Belemnite standard (PDB).

4. Results

4.1. Paleosol classification

Of the total thickness of the Stanleyville section (323 m), approximately 21% consists of pedogenically altered material. Three different paleosol morphologies were identified in the Stanleyville section of the Samba core (Figs. 3–4). Vertic Protosols are the most abundant paleosol type, whereas Vertisols and calcic Vertisols are much less common (Table 1).

4.1.1. Vertic Protosols

Seventy percent of the paleosols in the Stanleyville section are vertic Protosols. These paleosols are characterized by vertic features in weakly-developed profiles. Vertic Protosols are most often identified by the presence of clastic dikes in otherwise unmodified, homogenous matrix (Fig. 5). When clastic dikes are absent, these profiles may have poorly-developed slickensides, occasionally in conjunction with incipient angular blocky ped structure or wedge-shaped aggregates. Although clastic dikes help determine the upper contacts of many profiles, lower contacts are commonly difficult to distinguish due to weak morphological development of pedogenic features in

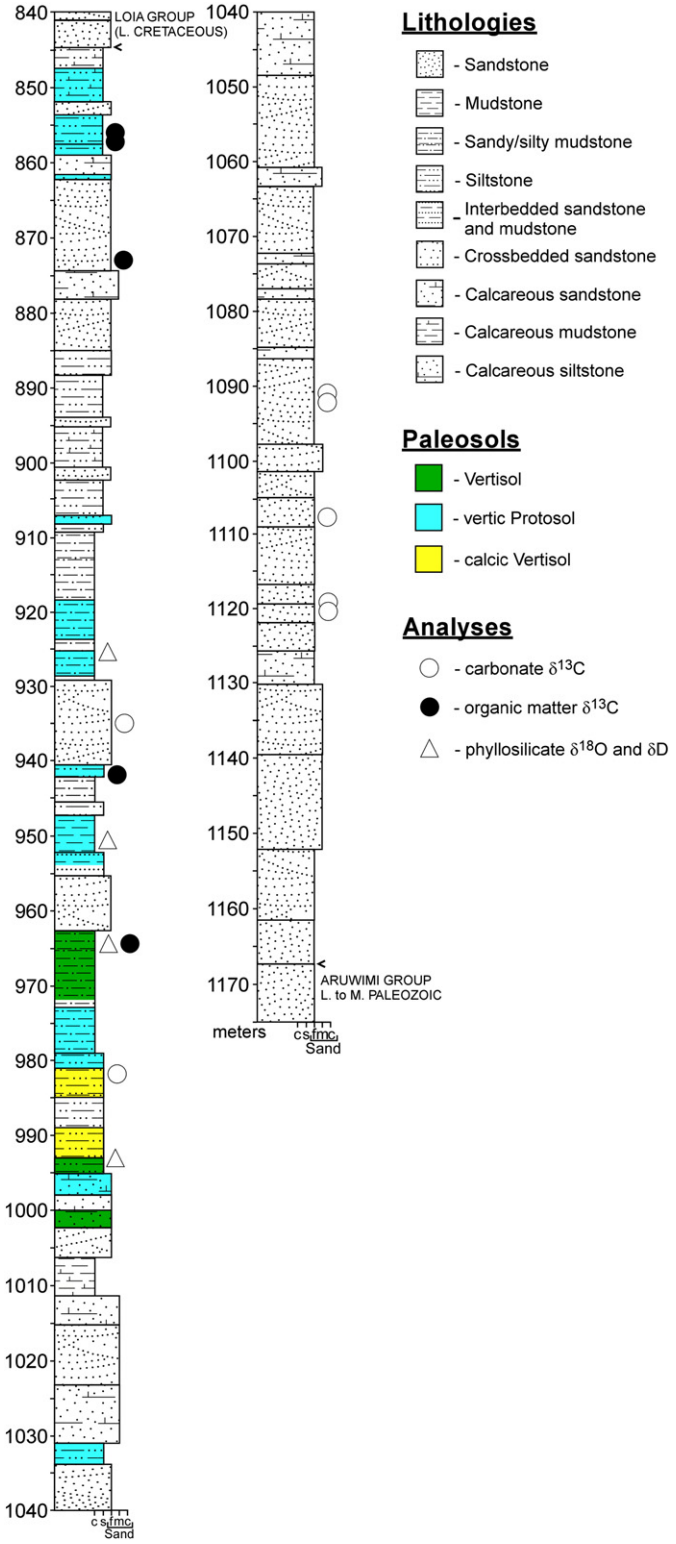

Fig. 3. Stratigraphic section of the Stanleyville Group in the Samba core showing distribution of paleosol types. Lithologies and measurements taken from Cahen et al. (1959). Paleosols are absent in the lower portion of the Stanleyville section.

the B-horizon. Profiles vary between one and several meters in thickness (Fig. 3). Vertic Protosols are spread throughout the paleosol-bearing portion of the Stanleyville Group and formed in a variety of lithologies. Vertic Protosols developed in fine-grained deposits such as mudstones typically have slickensides and evidence of ped

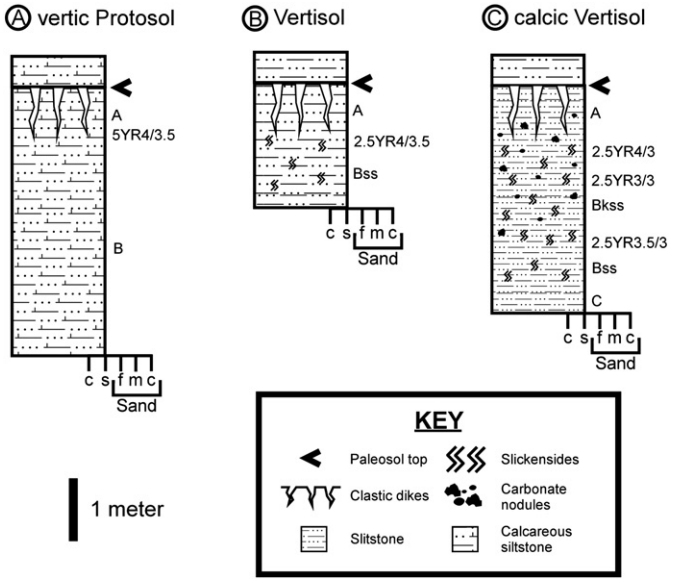

Fig. 4. Diagrammatic illustrations of representative paleosol profiles described from the Stanleyville Group.

structure. Profiles in coarser-grained deposits—siltstones and muddy sandstones—exhibit clastic dikes, but lack other pedogenic features.

4.1.2. Vertisols

Vertisols are a minor component (18%) of the Stanleyville section relative to vertic Protosols, with only three profiles observed (Fig. 3, Table 1). These paleosols are dominated by well-developed suites of vertic features. Each profile has clastic dikes at its upper contact and a well-defined Bss horizon. Stanleyville Vertisols developed in mudstone, siltstone, and muddy sandstone, but well-developed wedge-shaped ped structure was observed in only a single profile from the finest-grained deposit. Vertisol profiles in the Samba core range from 2 to 5 m and are not as thick on average as vertic Protosols. Nevertheless, the Stanleyville Vertisol profiles are more mature in terms of their morphological development.

4.1.3. Calcic Vertisols

Calcic Vertisols are the least abundant paleosol type in the Stanleyville Group, with only two profiles recorded (Fig. 3, Table 1). These paleosols possess Bkss horizons, containing both weakly-developed slickensides and pedogenic carbonate accumulations. Calcic Vertisol profiles are dominated by vertic features, including both clastic dikes and slickensides, while carbonate accumulations are a relatively minor component. Carbonate deposits formed as either discrete nodules (stage II Bk horizon; Gile et al., 1966) or diffuse, wispy seams of calcite (stage I Bk horizon; Gile et al., 1966). These paleosols developed in siltstones, and no ped structure is visible, despite the presence of slickensides. Both calcic Vertisols in the Stanleyville section are between 2 and 3 m thick.

Table 1
Abundances of paleosol types within the Stanleyville Group.

Paleosol type	# of profiles	% of profiles	% of section thickness
Vertic Protosol	12	70	14
Vertisol	3	18	4
Calcic Vertisol	2	12	3

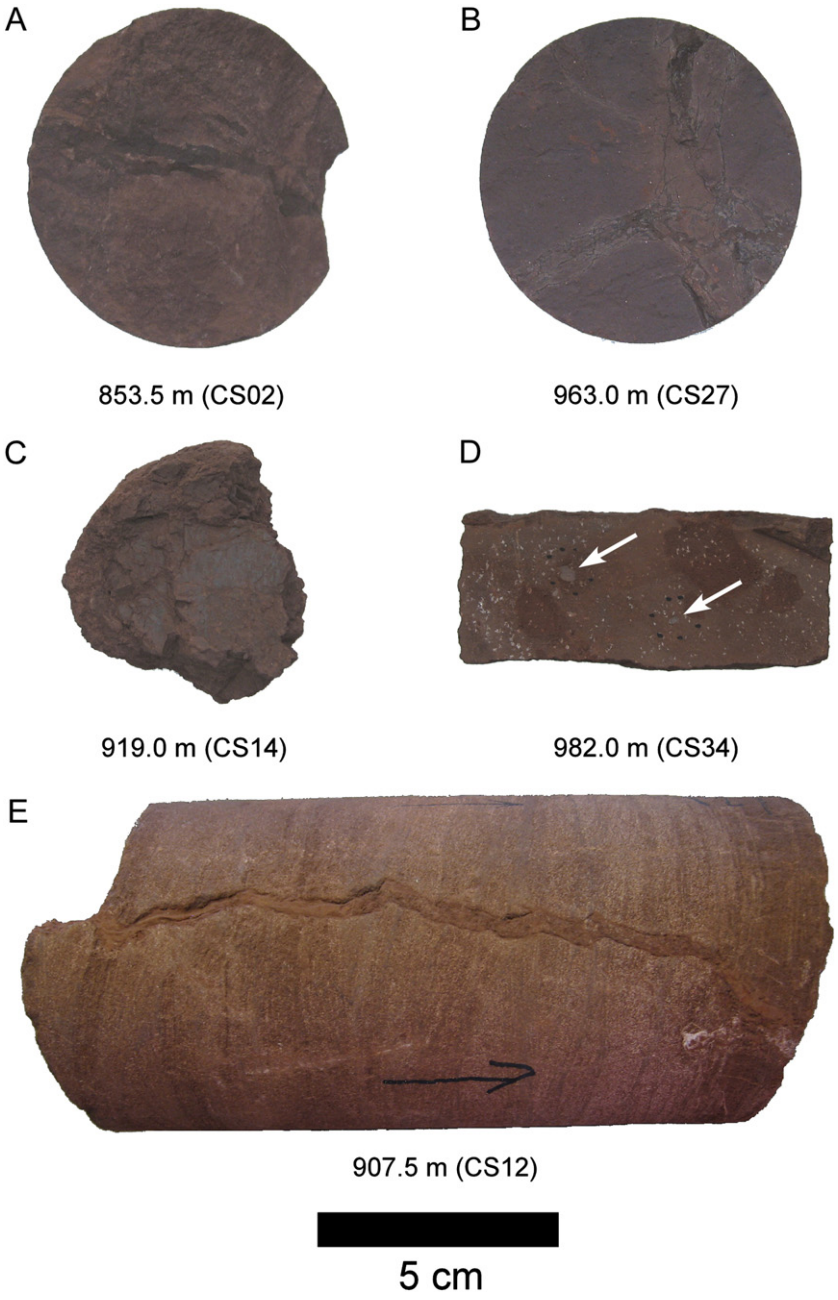

Fig. 5. Photos of pedogenic features observed in the Stanleyville Group. (A) Clastic dikes from a vertic Protosol at 853.5 m depth, (B) clastic dikes from a Vertisol at 963.0 m depth, (C) slickensides from a vertic Protosol at 919.0 m depth, (D) carbonate nodules from a calcic Vertisol at 982.0 m depth, (E) clastic dike from a vertic Protosol at 907.5 m depth.

4.2. Stratigraphic distribution of paleosols

The highest concentration and diversity of paleosols in the Stanleyville Group occurs within the interval containing the Jurassic–Cretaceous boundary (1009–942 m; Cahen, 1983). Uncertainty regarding the exact location of the boundary within this interval makes it difficult to determine which paleosols are Upper Jurassic and which are Lower Cretaceous. Most of the observed paleosols occur in the upper half of the Stanleyville section, extending from approximately 1035 m to 845 m depth. Below 1035 m, the Stanleyville consists of relatively coarse-grained, sandy deposits devoid of pedogenic features. These lower fluvial sandstones are characterized by horizontal bedding and, less commonly, crossbedding. Above 1035 m, finer-grained deposits increase in abundance, and paleosol profiles occur sporadically. Vertic Protosols are scattered throughout the paleosol-bearing part of the section. Only a small interval extending from 1005 m to 950 m depth contains more mature Vertisol profiles, some containing traces of pedogenic calcite (Fig. 3). Overall, pedogenic alteration of Stanleyville strata is rather limited.

4.3. X-ray diffraction-analysis of paleosol matrix samples

Powdered samples from the >2 μm coarse size fraction contain a high abundance of the zeolite analcime, with characteristic peaks at 5.60 Å and 3.42 Å. For potentially Upper Jurassic samples collected between 1031.0 m and 942.5 m depth, estimates of analcime abundance range from 9% to 57%, with an average of 31% (Fig. 6). Analcime abundance varies considerably throughout both the Upper Jurassic and Lower Cretaceous parts of the Stanleyville section, and there is no discernable correlation with lithology or paleosol type. Other common minerals in the matrix coarse fraction include quartz and

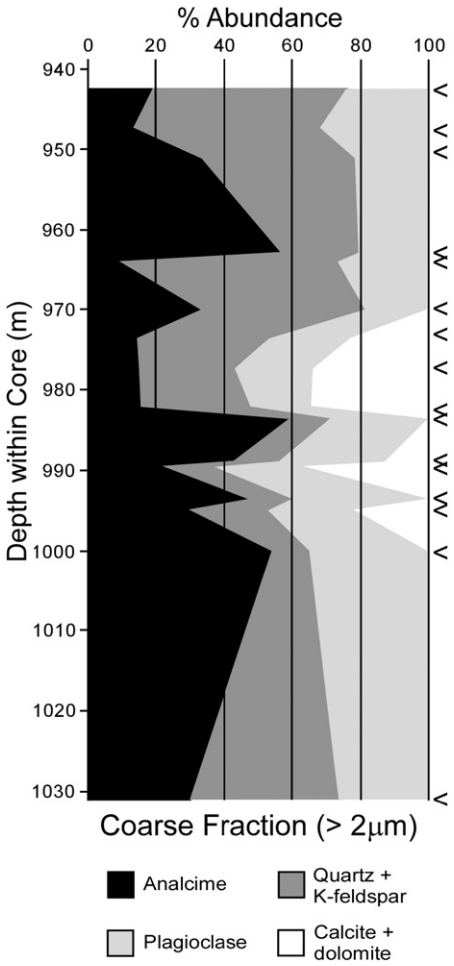

Fig. 6. Relative abundance of primary minerals in coarse fraction (>2 μm) samples collected from the Samba core between 1031.0 m and 942.5 m depth. Analcime is a major component of the >2 μm size fraction, with abundances ranging from 9% to 59%. Abundance estimates derived from area measurements of 001 peaks in powder diffraction patterns. Symbols along the right margin denote stratigraphic positions of matrix samples analyzed.

feldspar, and some samples also contain minor amounts of pedogenic calcite or dolomite that could not be avoided in the sampling process.

The clay mineralogy (<2 μm) of a sample from a representative Vertisol at 964.0 m (Fig. 3) is summarized in Fig. 7. The total clay fraction is dominated by illite and mixed-layer illite–smectite. Small peaks at 7.10 Å and 3.52 Å indicate the presence of trace amounts of kaolinite, whereas peaks at 4.49 Å and 4.26 Å are indicative of palygorskite. The primary peak for palygorskite, which typically occurs at 10.4 Å, is obscured by the wide peaks of illite and mixed-layer illite–smectite around 10.0–11.5 Å. Traces of analcime occur occasionally in the total clay fraction throughout the section. The fine clay fraction (<0.2 μm) from the same sample (CS29) consists entirely of illite and mixed-layer illite–smectite, with no traces of kaolinite or palygorskite. Analyses of other samples from different paleosol profiles in the Samba core show similar patterns, although some also contain minor amounts of smectite (Fig. 8).

Analysis of the stratigraphic distribution of clay minerals within the Stanleyville Group reveals higher concentrations of smectite and mixed-layer illite–smectite below approximately 915 m depth (Fig. 8). This interval of greater smectite abundance is resolvable in both the total and fine clay fractions. Above 915 m, in the Lower Cretaceous part of the section, smectite occurs in only small amounts, and the clay mineral assemblage is dominated by illite with only minor amounts of kaolinite. Palygorskite-bearing samples are restricted to the interval of higher smectite abundance in the lower two thirds of the section (>915 m; Fig. 3). Most of the paleosols (76%) fall within the smectite and palygorskite-bearing zone below 915 m, with only four profiles (24%) located above this zone.

4.4. Oxygen and hydrogen isotope analysis of clay minerals

The $\delta^{18}O$ and δD values measured from the fine clay fractions of four paleosol matrix samples are given in Table 2. Three samples from the Jurassic–Cretaceous boundary interval have $\delta^{18}O$ values between +22.3‰ and +25.4‰ SMOW and δD values between −44.4‰ and −39.6‰ SMOW. The fourth sample, from Lower Cretaceous strata in the upper part of the section (Cahen, 1983), has a $\delta^{18}O$ value of +25.4‰ and a δD value of −48.5‰.

4.5. Carbon isotope analysis of carbonates and plant-derived organic matter from the Stanleyville Group

Of the seven carbonate specimens sampled from the Samba core, only one is suitable for use in estimation of soil CO_2 production (Ekart et al., 1999; Tabor et al., 2004; Sheldon and Tabor, 2009). This micritic calcite nodule, collected from a calcic Vertisol in Upper Jurassic–Lower Cretaceous strata at 982.0 m depth (Fig. 3), has a $\delta^{13}C$ value of −6.8‰ PDB (Table 3). All other carbonate samples from the Stanleyville section were collected from coarse-grained fluvial deposits rather than paleosols, and although they were likely formed by pedogenic processes, they are detrital sedimentary clasts and therefore inappropriate for use in CO_2 production calculations (Ekart et al., 1999; Tabor et al., 2004; Sheldon and Tabor, 2009). The $\delta^{13}C$ values of these six samples are 2.6‰ more positive, on average, than that of the nodule collected from the calcic Vertisol (Table 3).

Five organic matter samples were analyzed for determination of $\delta^{13}C$ values. Three of these samples come from the Lower Cretaceous part of the Stanleyville section, and two samples were collected from the Jurassic–Cretaceous boundary interval between 1009 m and 942 m depth (Cahen, 1983). One of the samples (CS03) was composed of carbonized woody material, but the rest comprised small particles of unidentifiable organic matter. Carbon isotope values for these organics range from −24.8‰ and −23.2‰ PDB, with an average of −24.3‰ (Table 3).

4.6. Carbon isotope analysis of plant-derived organic matter from the Morrison Formation

Carbonized plant material is exceedingly scarce within the Morrison Formation, so despite careful inspection of over 1000 m of section at several different localities, only four organic samples were recovered from three sites. One sample from Montana (MD020) consists of carbonized woody material, and the rest are composed of particles of organic matter suspended in clastic matrix. The $\delta^{13}C$ values of these samples range from −22.3‰ to −18.7‰ PDB, with an average of −21.0‰ (Table 4).

5. Discussion

5.1. Paleoclimate conditions based on paleosol morphology

Slickensides and abundant clastic dikes observed in Stanleyville paleosols are indicative of variations in moisture availability. Vertic features in modern soil profiles are formed by shrink-and-swell processes resulting from cyclical wetting and drying (Wilding and Tessier, 1988; Coulombe et al., 1996). Slickensides observed in Stanleyville paleosols are typically poorly developed because of the high silt content of the mudstones, whereas clastic dikes are quite deep, commonly extending >0.5 m from the paleosol surface. The depth of cracking in modern Vertisols is directly related to intensity of desiccation within the soil profile (Zein el Abedine and Robinson, 1971; Dasog et al.,

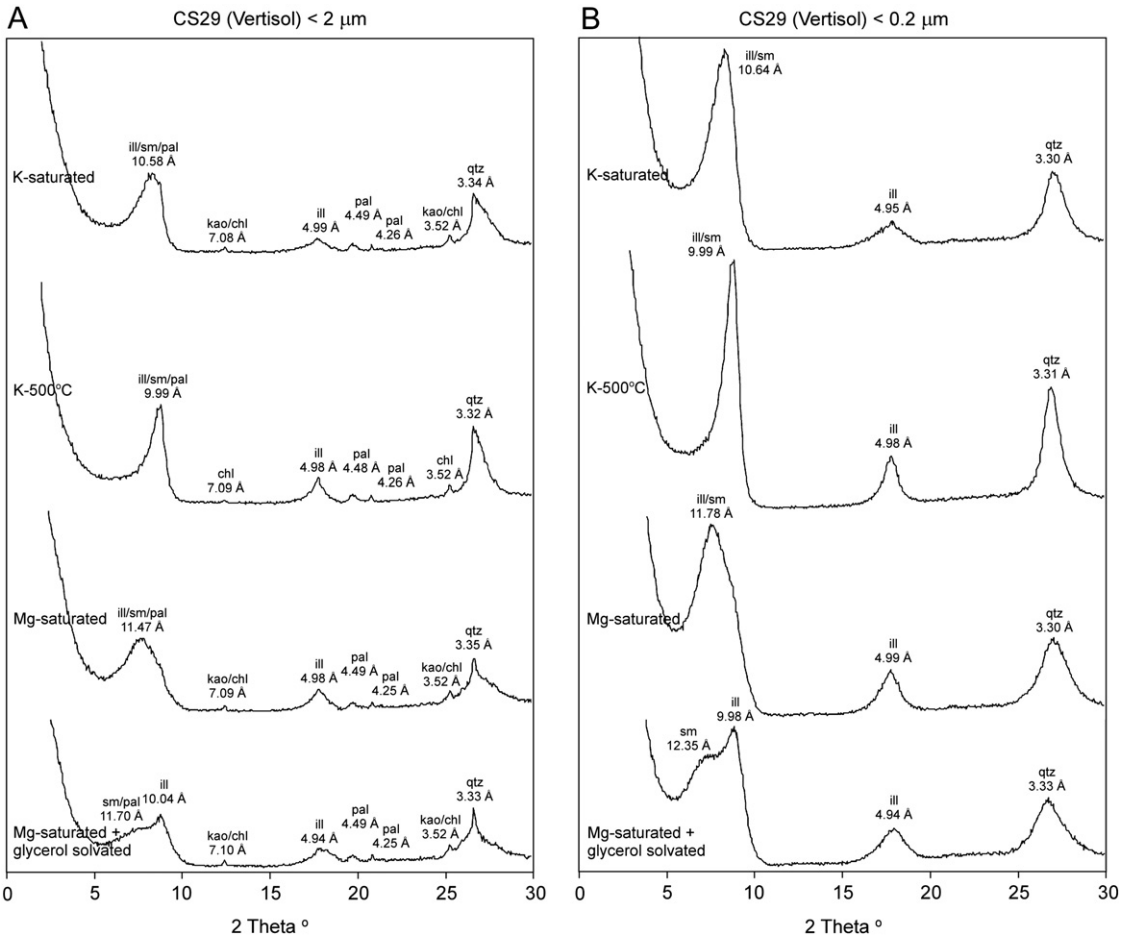

Fig. 7. XRD spectra for oriented aggregates of the total clay fraction (<2 μm) and fine clay fraction (<0.2 μm) from a Vertisol at 964.0 m depth containing illite, mixed-layer illite/smectite, and trace amounts of palygorskite.

1988), where the distal termination of soil cracks signals the transition from dry to moist soil matrix (Dudal and Eswaran, 1988). Consequently, the deep penetration of clastic dikes in the Stanleyville paleosols may reflect thick zones of low soil moisture in the upper parts of the soil profiles, related to intense desiccation. Although other common vertic features, such as mukkara structure and gilgai microrelief, were not identified in the Stanleyville paleosol profiles, the relatively large scale of these features makes them difficult to detect in the small cross-section of the drill core. The small diameter of the core may also have allowed some poorly-developed paleosols (e.g., non-vertic Protosols) to escape detection, although such types of profiles would provide little additional paleoclimatic information.

The absence of paleosol profiles in the lower part of the Stanleyville Group (Fig. 3) is likely related to the coarse-grained texture and higher sedimentation rates of the fluvial channel deposits. Although paleosols developed within finer-grained mudstones in the upper part of the section, even these profiles typically lack well-developed horizonation and pedogenic structure (Figs. 3–4). Many of the thicker paleosol profiles, especially Vertisols and vertic Protosols, appear to be cumulic in nature (*sensu* Marriott and Wright, 1993), suggesting that some Stanleyville soil-forming environments were characterized by constant sedimentation rates and relatively slow aggradation. Conversely, thick vertic Protosols characterized by the presence of clastic dikes alone suggest pulses of more rapid sedimentation. Generally weak morphological development among the majority of the Stanleyville paleosols is likely related to reduced chemical weathering rates and low biological productivity in the soil, both of which are characteristic of arid environments (Melillo et al., 1993; Sellwood and Price, 1993; Mack and James, 1994; Churkina and Running, 1998; Nemani et al., 2003; Bradford et al., 2006). Notably, no evidence of rooting (e.g., rhizoliths or root traces) was observed in any of the paleosol profiles in the Stanleyville Group. If the lack of root structures in Stanleyville paleosols is attributable to absence of significant vegetation, this provides further support for interpretation of Stanleyville paleoenvironments as arid and inhospitable.

5.2. Paleoclimate conditions based on matrix mineralogy

Earlier mineralogical analysis of sedimentary matrix in the Stanleyville section of the Samba core indicated that beds above approximately 1100 m were dominated by analcime (Vanderstappen and Verbeek, 1964). The analcime present in the Stanleyville deposits was initially suggested to be an alteration product of volcanic materials (Vernet, 1961), but subsequent analyses concluded that a non-volcanic origin for the analcime was more likely (Vanderstappen and Verbeek, 1964). XRD analysis reveals trace amounts of analcime in the Stanleyville clay assemblages (<2 μm fraction), but the bulk of the analcime is concentrated in the >2 μm size fraction. Sedimentary analcime is associated with arid environments, forming in saline, alkaline brines of lacustrine and playa settings by crystallization from gelatinous aluminosilicates at or below the water table (Hartley et al., 1991; English, 2001; Do Campo et al., 2007). The alumina and silica necessary for analcime crystallization may be derived from decomposition of either volcaniclastic material, feldspars, or clay minerals that are unstable in sodium-rich brines depleted in silicon and aluminum (English, 2001).

Soil-formed palygorskite develops in arid climates, often in association with gypsum-bearing parent materials such as those derived from shallow, saline lakes or lagoons (Khademi and Mermut, 1998).

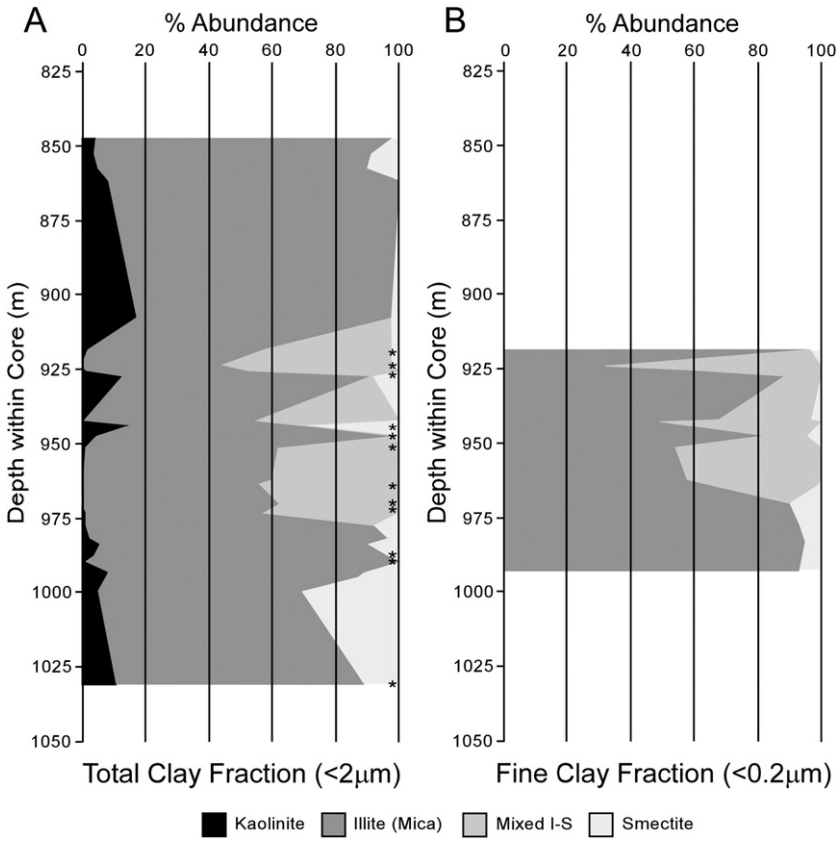

Fig. 8. Relative abundance of clay minerals from the Stanleyville section of the Samba core. The interval below 915 m is characterized by higher abundance of smectite and the presence of palygorskite, indicated with an asterisk. Palygorskite is absent above 915 m in the Lower Cretaceous part of the Stanleyville Group, but analcime occurs in the total clay fraction in trace amounts throughout the section.

Modern palygorskite-bearing soils are often saturated by saline groundwater (Singer, 1984; Curtis, 1990). Alternatively, non-pedogenic palygorskite may precipitate from alkaline brines in lacustrine or shallow marine environments (Callen, 1984) and be inherited by soil profiles that later overprint lacustrine strata within an arid climatic setting. Humid climatic conditions not only inhibit formation of pedogenic palygorskite, but also cause dissolution and removal of palygorskite from soil profiles (Singer, 1984). Therefore, the occurrence of palygorskite in the clay mineral assemblages of the Stanleyville paleosols strongly suggests arid climatic conditions.

Near 1011 m depth in the core are several seams of satin spar calcite with a medial scar, indicating replacement of gypsum. These seams formed between thin layers of lacustrine clay with alternating light and dark banding. The presence of analcime, palygorskite, and replaced gypsum in the Upper Jurassic part of the Stanleyville Group is consistent with hot, arid conditions and deposition in ephemeral fluvial and saline lacustrine paleoenvironments. The abrupt disappearance of palygorskite and the decrease in smectite, which is also typical of dry environments (Birkeland, 1999), at approximately 915 m may reflect a climatic shift toward more humid conditions in the Early Cretaceous.

Table 2
Measured $\delta^{18}O$ and δD values of phyllosilicates and mean annual soil temperature estimates for the Stanleyville Group. These temperatures should be considered maximum estimates due to errors resulting from variable sample composition.

Sample	Depth (m)	Paleosol type	Age	$\delta^{18}O$ (‰SMOW)	δD (‰SMOW)	Temperature (°C) ± 3°
CS16	925.5	Vertic Protosol	Lower Cretaceous	+25.4	−48.5	23
CS25	951.0	Vertic Protosol	U. Jurassic–L. Cretaceous	+22.9	−44.2	35
CS29	964.0	Vertisol	U. Jurassic–L. Cretaceous	+25.4	−44.4	25
CS39	993.5	Vertisol	U. Jurassic–L. Cretaceous	+22.3	−39.6	40

Table 3
Carbon isotope data for carbonates (n = 7) and plant-derived organic matter (n = 5) from the Stanleyville Group. CS34 is the only carbonate sample deemed appropriate for use with the CO_2 paleobarometer. Of the organic matter collected and analyzed, only samples CS21 and CS29 are potentially Upper Jurassic in age. CS03 consists of carbonized woody material, but all other organic samples are fine particulate matter derived from bulk matrix samples.

Carbonate nodules			
Sample	Depth (m)	Age	$\delta^{13}C$ (‰PDB)
CS18	935.0	Lower Cretaceous	−2.59
CS34	982.0	Upper Jurassic–Lower Cretaceous	−6.83
CS54	1091.0	Upper Jurassic	−4.07
CS55	1092.0	Upper Jurassic	−5.15
CS56	1108.0	Upper Jurassic	−4.80
CS57	1119.5	Upper Jurassic	−4.17
CS58	1120.5	Upper Jurassic	−4.31
Organic matter			
CS03	856.5	Lower Cretaceous	−23.16
CS04	857.5	Lower Cretaceous	−24.67
CS09	874.0	Lower Cretaceous	−24.81
CS21	942.0	Upper Jurassic–Lower Cretaceous	−24.63
CS29	964.0	Upper Jurassic–Lower Cretaceous	−24.22

Table 4
Carbon isotope data for plant-derived organic matter (n = 4) from three localities in the Morrison Formation. Average $\delta^{13}C$ value for all samples is −21.0‰. GR = Ghost Ranch, NM; MD = Bridger, MT; SH = Shell, WY.

Sample	Weight % C	$\delta^{13}C$ (‰ PDB)	Material
GR014	46.1	−21.99	Bulk
GR016A	1.4	−18.68	Bulk
MD020	53.5	−21.20	Wood
SH019	2.9	−22.28	Bulk

5.3. Paleotemperature proxy

Measured $\delta^{18}O$ and δD values of clay minerals were used to estimate average annual soil paleotemperature using the equation derived by Delgado and Reyes (1996), rearranged to isolate the temperature variable:

$$T_K = \sqrt{\frac{3.54 \times 10^6}{\delta^{18}O - 0.125\delta D + 8.95}} \quad (1)$$

Three Upper Jurassic–Lower Cretaceous samples produced soil temperature estimates ranging from 25 °C to 40 °C ± 3 °C (Table 2), with an average of 33 °C (1σ = 7.6 °C). A Lower Cretaceous sample produced an estimate of 23 °C ± 3 °C. The clay minerals used in this analysis are assumed to have formed in isotopic equilibrium with meteoric waters with $\delta^{18}O$ values between 0‰ and +1‰ SMOW (Fig. 9); however, given the high temperatures suggested by these estimates and the presence of the arid environmental indicators palygorskite and analcime, the Stanleyville clay mineral assemblages may have formed in the presence of waters subjected to evaporative effects. The isotopic composition of surface waters that have undergone intensive evaporation reflects kinetic, rather than equilibrium, fractionation (Savin and Hsieh, 1998). On a plot of $\delta^{18}O$ vs. δD values, heavily evaporated waters are shifted to the right of the meteoric water line (Fig. 9; Savin and Hsieh, 1998). If the clay minerals analyzed here formed from waters evaporatively enriched in ^{18}O and deuterium, the measured $\delta^{18}O$ and δD values would correspond to even higher paleotemperatures.

It is important to note that the temperature equation presented by Delgado and Reyes (1996) was developed for smectite, and the clay mineral samples analyzed here contain variable amounts of kaolinite and illite in addition to smectite. The temperature dependence functions for the fractionation factors of kaolinite and mixed-layer illite–smectite differ from that of smectite (Capuano, 1992; Savin and Hsieh, 1998), such that the paleotemperature estimates produced here using the Delgado and Reyes equation are slight (<3 °C) overestimates. These paleotemperature estimates should be considered maximum average annual soil temperatures. Yet, evidence has been found for similarly high temperatures based on Δ^{47} measurements of Quaternary soil and paleosol calcite (Passey et al., 2010), as well as Permian-age fluid inclusions within continental evaporites (Benison and Goldstein, 1999). The paleotemperature estimates generated here are consistent with soil temperatures measured in modern, dry tropical sites.

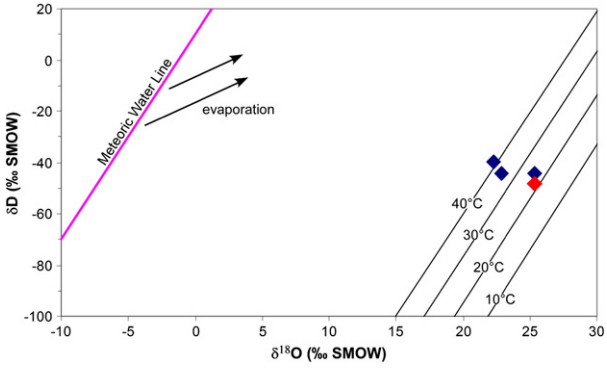

Fig. 9. Plot of $\delta^{18}O$ vs. δD values for selected clay mineral samples from the Stanleyville Group. The meteoric water line is shown at left, and the isotherms on the right represent potential compositions of smectite formed in equilibrium with meteoric waters at different temperatures. Blue markers represent compositions of Upper Jurassic–Lower Cretaceous samples, and the red marker represents a Lower Cretaceous sample. The measured isotopic compositions of the three Jurassic–Cretaceous samples suggest an upper limit for average annual soil paleotemperature between 35 °C and 40 °C.

5.4. Estimation of soil CO_2 production

The $\delta^{13}C$ values of pedogenic carbonate and plant-derived organic matter collected from the Stanleyville section of the Samba core and the Morrison Formation permit estimates and comparison of Late Jurassic soil CO_2 concentrations between these two areas. These calculations require (1) calcite and organic matter $\delta^{13}C$ values presented here from the Samba core (Table 3), (2) organic matter $\delta^{13}C$ values from Morrison Formation samples presented here (Table 4), and (3) calcite $\delta^{13}C$ values from Morrison Formation samples presented in Ekart et al. (1999). Carbon isotope fractionation for $CO_{2(g)}$—calcite was calculated using the equation experimentally derived by Romanek et al. (1992):

$$\varepsilon_{cc-CO_2} = 11.98 - 0.12 * T_{\circ C} \quad (2)$$

where $\varepsilon_{cc\text{-}CO2}$ is the calcite-$CO_{2(g)}$ enrichment factor. Based on the range of temperatures estimated from paleosol phyllosilicate $\delta^{18}O$ and δD values (Table 2), $CO_{2(g)}$–calcite carbon isotope fractionation factors were calculated at 5 °C increments between 20 °C and 35 °C (Table 5). The equation developed by Cerling (1991) and reformulated by Ekart et al. (1999) is rearranged to isolate the soil CO_2 production variable S (z) and used to estimate in-situ soil CO_2 production:

$$S(z) = C_A \frac{\delta^{13}C_A - \delta^{13}C_S}{\delta^{13}C_S - 1.0044\delta^{13}C_O - 4.4} \quad (3)$$

where C_A is the concentration of CO_2 in the atmosphere, $\delta^{13}C_A$ is the $\delta^{13}C$ value of atmospheric CO_2, $\delta^{13}C_S$ is the $\delta^{13}C$ value of soil CO_2, $\delta^{13}C_O$ is the $\delta^{13}C$ value of soil-respired CO_2 (produced by in-situ soil processes), and S(z) is the concentration of soil-respired CO_2, equal to $p(CO_2)_{soil} - p(CO_2)_{atm}$. All pedogenic carbonates were collected from

Table 5
Soil CO_2 production estimates calculated using Upper Jurassic samples from the Stanleyville Group and the Morrison Formation. Carbon isotope fractionation factors were calculated at 5 °C increments between 20 °C and 35 °C using the equation derived by Romanek et al. (1992). S(z) values calculated from the Stanleyville carbonate sample (CS34, 982.0 m depth) use the $\delta^{13}C$ value of the nearest plant-derived organic matter in the Samba core (−24.2‰) to represent soil-respired CO_2 ($\delta^{13}C_O$). The average $\delta^{13}C_{cc}$ value reported by Ekart et al. (1999) (−6.2‰ ± 1.0‰ 1σ) was used in conjunction with the average $\delta^{13}C$ value of the organic samples in Table 4 (−21.0‰ ± 1.6‰ 1σ) to generate soil CO_2 production estimates for the Morrison Formation (EKM). $\delta^{13}C_{Atm} = -6.7$‰ PDB, C_A = 1450 ppmV (5X PAL).

Sample	Temp (°C)	$\varepsilon_{CO2\text{-}cc}$	$\delta^{13}C_{cc}$ (‰ PDB)	$\delta^{13}C_S$ (‰ PDB)	$\delta^{13}C_O$ (‰ PDB)	S(z) (ppmV)
CS34	20	−9.6	−6.8	−16.4	−24.2	4011
CS34	25	−9.0	−6.8	−15.8	−24.2	3213
CS34	30	−8.4	−6.8	−15.2	−24.2	2618
CS34	35	−7.8	−6.8	−14.6	−24.2	2158
EKM	20	−9.6	−6.2	−15.8	−21.0	14,786
EKM	25	−9.0	−6.2	−15.2	−21.0	8259
EKM	30	−8.4	−6.2	−14.6	−21.0	5474
EKM	35	−7.8	−6.2	−14.0	−21.0	3931

depths at least 50 cm beneath the paleosol surface, likely below the zone where mixing of atmospheric and soil-respired CO_2 produces steep gradients in concentration and isotopic composition of soil CO_2 (Cerling and Quade, 1993; Ekart et al., 1999). Using marine carbonate values reported in Veizer et al. (1999) and assuming a constant offset of −8‰ between surface ocean carbonates and the atmosphere (Ekart et al., 1999), Late Jurassic atmospheric $\delta^{13}C$ is estimated at −6.7‰ PDB.

$\delta^{13}C_S$ is calculated from measured calcite $\delta^{13}C$ values based on assumed temperatures of crystallization in the soil (Table 5). Considering that the Morrison Formation and Upper Jurassic Stanleyville Group paleosol profiles are coeval soil systems and that atmospheric CO_2 has a short residence time in Earth's troposphere and, therefore, is well mixed, atmospheric pCO_2 (C_A in Eq. (3)) should be identical for estimates of S(z) in both the Morrison and Stanleyville paleosols. It is not necessary to specify the actual value of C_A because S(z) values for the Morrison Formation and Stanleyville Group may be expressed as a ratio (i.e., $S(z)_{Morrison}/C_{Aglobal}$; $S(z)_{Stanleyville}/C_{Aglobal}$; $C_{Aglobal}/C_{Aglobal} = 1$). For demonstration purposes, however, it is useful to input some value of C_A in order to estimate concentrations of S(z) in units of ppmV. Most CO_2 models agree that Late Jurassic atmospheric pCO_2 was substantially higher than modern (Budyko et al., 1985; Berner and Kothavala, 2001; Berner, 2006a, 2006b). The most recent version of the GEOCARBSULF model (Berner, 2008) produces estimates of atmospheric pCO_2 for the Late Jurassic (500–1000 ppmV) that are lower than those derived from independent proxies (Royer, 2006). 5X PAL (PAL = 290 ppmV) was selected as the C_A value in Eq. (3) because it is intermediate between the estimates calculated from recent carbon mass flux models and independent proxies (Royer, 2006; Berner, 2008).

$\delta^{13}C$ values of fossilized plant material collected from the Stanleyville Group (Table 3) and the Morrison Formation (Table 4) are used as input values for the $\delta^{13}C$ composition of soil-respired CO_2 ($\delta^{13}C_O$ in Eq. (3)). Using this approach, the $\delta^{13}C_S$ values calculated from the pedogenic carbonate $\delta^{13}C$ value in the Stanleyville section (CS34, 982 m) are matched with the $\delta^{13}C$ value of the stratigraphically-nearest organic material (CS29, 964 m). The average of the Morrison Formation organic $\delta^{13}C$ values in Table 4 (−21.0‰ ± 1.6‰ 1σ, n = 4) was used in conjunction with the average $\delta^{13}C$ value of Morrison Formation pedogenic carbonate samples reported by Ekart et al. (1999) (−6.2‰ ± 1.0‰ 1σ, n = 63). Soil CO_2 production, or S(z), estimates resulting from this calculation in the Stanleyville Group range from ~4000 ppmV for a temperature of 20 °C to ~2200 ppmV at 35 °C, whereas estimates for the Morrison Formation range from ~14,800 ppmV (20 °C) to ~3900 ppmV (35 °C) (Table 5). The averages for each of the sets of four S(z) values calculated at different temperatures for the Stanleyville Group and Morrison Formation are determined to be significantly different using a separate-variance *t* test (α = 0.10). Estimates of S(z) calculated at 35 °C for the Stanleyville sample are probably more realistic than estimates calculated at 20 °C, considering the temperature estimates derived here from paleosol phyllosilicate samples.

Soil-respired CO_2 appears to be strongly linked with actual evaporation lost from the soil through biological production, and biological production is strongly correlated with mean annual precipitation (Witcamp, 1966; Garrett and Cox, 1973; Edwards, 1975; Lieth, 1975; Brooke et al., 1983; Buyanovsky and Wagner, 1983). Therefore, lower soil CO_2 production estimates for the Stanleyville Group relative to the Morrison Formation are consistent with arid Late Jurassic climate conditions inferred for the Congo Basin from paleosol morphology and matrix mineralogy.

5.5. Comparison with other Upper Jurassic continental deposits in Africa

Upper Jurassic continental deposits are exposed rarely in Africa. Large swaths of the northern and eastern continental margins were submerged by epicontinental seas during the Late Jurassic (Guiraud et al., 2005), and erosional processes dominated the continental interior (Arkell, 1956). Of the few Upper Jurassic terrestrial successions preserved in Africa, perhaps the best-known is the Tendaguru Formation of Tanzania (Bussert et al., 2009). Upper Jurassic continental strata with reasonable age control are also exposed in Algeria (Busson and Cornée, 1991), Ethiopia (Assefa, 1991; Goodwin et al., 1999), Mali (Bamford et al., 2002), Niger (Ginsburg et al., 1966; Alessandrello and Teruzzi, 1989), Somalia (Angelucci et al., 1983), Sudan (Awad and Schrank, 1993), Tunisia (Anderson et al., 2007), and Zimbabwe (Bond and Bromley, 1970; Raath and McIntosh, 1987).

Paleoclimate information is not available for the Upper Jurassic–Lower Cretaceous beds of the Continental Intercalaire in eastern Niger (Ginsburg et al., 1966; Alessandrello and Teruzzi, 1989) or the Upper Jurassic continental deposits in southern Tunisia (Benton et al., 2000; Anderson et al., 2007). Dinosaur-bearing strata of the Kadzi Formation in northern Zimbabwe are similarly lacking reports of paleoclimate indicators. The Gokwe Formation of northwestern Zimbabwe and other nearby deposits that are potentially correlative with the Kadzi Formation retain evidence of shallow, alkaline lacustrine paleoenvironments with thin evaporite layers present in some areas (Bond and Bromley, 1970; Cooper, 1988; Ait-Kaci Ahmed et al., 2004). Sedimentological and taphonomic evidence of intermittent flooding implies that rainfall patterns during deposition of the Gokwe Formation were strongly seasonal (Bond and Bromley, 1970). Fluvial deposits in the Continental Intercalaire of northeastern Mali contain large amounts of silicified wood, analysis of which suggests a hot and arid isothermal climate with adequate water to support large conifers (Bamford et al., 2002).

Available evidence suggests that Late Jurassic paleoclimatic conditions in Ethiopia, Somalia, and Sudan were relatively arid. The Upper Jurassic Mugher Mudstone in central Ethiopia consists of marginal marine deposits overlain by fine-grained fluvial sediments (Assefa, 1991; Schmidt and Werner, 1998). These rocks contain a diverse vertebrate fauna, including fishes, turtles, crocodilians, theropod and sauropod dinosaurs, and mammals (Goodwin et al., 1999; Clemens et al., 2007). Sedimentary and pedogenic climate indicators imply hot, dry conditions with seasonal precipitation (Assefa, 1991; Schmidt and Werner, 1998). Upper Jurassic floral remains from western Sudan are also interpreted as evidence of arid to semi-arid conditions (Awad and Schrank,

Table 6
Upper Jurassic continental deposits of Africa and paleoclimatic conditions inferred from published interpretations and reports of sedimentological data. Some successions extend into the Cretaceous. Paleolatitudes were estimated using the PointTracker program (Scotese, 2002). Locality numbers correspond to Fig. 10.

Locality number	Location	Stratigraphy	Paleolatitude	Paleoclimate	Reference
1	Algeria	Taouratine Formation	17°N	Humid	Busson and Cornée, 1991
2	Ethiopia	Mugher Mudstone	12°S	Arid	Assefa, 1991
3	Mali	Continental Intercalaire	11°N	Intermediate	Bamford et al., 2002
4	Niger	Assaouas Sandstones	8°N	NA	Alessandrello and Teruzzi, 1989
5	Somalia	Garbaharre Formation	19°S	arid	Angelucci et al., 1983
6	Sudan	Abu Gin Formation	5°S	Arid	Awad and Shrank, 1993
7	Tanzania	Tendaguru formation	30°S	Humid	Aberhan et al., 2002
8	Tunisia	Asfer Group	20°N	NA	Anderson et al., 2007
9	N Zimbabwe	Kadzi Formation	32°S	NA	Raath and McIntosh, 1987
10	W Zimbabwe	Gokwe Formation	33°S	Intermediate	Bond and Bromley, 1970
11	DRC	Stanleyville Group	13°S	Arid	This study

1993). Contemporary marginal marine deposits in Somalia contain gypsum layers consistent with aridity (Angelucci et al., 1983).

In contrast, the paleoclimatic setting of the Tendaguru Formation is reconstructed as tropical to sub-tropical with pronounced seasonality of rainfall (Aberhan et al., 2002). Middle–Upper Jurassic strata in eastern Algeria are also interpreted as evidence of warm, humid climate (Busson and Cornée, 1991). Kaolinite-dominated clay assemblages and ferruginous crusts suggest high weathering rates typical of tropical climates (Busson and Cornée, 1991). These units comprise both palustrine and fluvial deposits and contain abundant fragments of wood and vertebrate fossil material (Busson and Cornée, 1991).

Although the paleoclimate categories applied here (arid, humid, intermediate) are rather coarse and sometimes based on limited data, paleoclimate indicators suggest that paleogeographic zones with distinctly different climate patterns were present on the Late Jurassic African continent (Fig. 10). Sites where annual precipitation is inferred to be roughly equivalent to, or greater than, evapotranspiration occur in coastal areas near the equator and at approximately 30°S paleolatitude. Sites with stronger evidence of aridity are clustered in a low-latitude belt stretching from 5°S to 20°S paleolatitude.

5.6. Comparison with global studies of Late Jurassic climate

The results of this study provide an important reference point for comparison with large-scale reconstructions of global paleoclimate in the Late Jurassic. Global studies have utilized a variety of techniques to interpret paleoclimatic conditions, including climate modeling (Sellwood and Valdes, 2008), phytogeographic analysis (Rees et al., 2000), and geospatial analysis of climatically-sensitive sedimentary deposits (Hallam, 1984). Interpretation of central African paleoclimatic conditions as hot and arid with a small amount of seasonal precipitation is consistent with the outputs of a succession of general circulation models (Valdes and Sellwood, 1992; Sellwood and Valdes, 2006, 2008). In contrast to the arid continental interior, the Tethyan coastlines of Africa are often modeled as areas of high seasonal rainfall (Valdes and Sellwood, 1992: Fig. 4; Sellwood and Valdes, 2006: Fig. 3C–D, 2008: Fig. 5A). The paleogeographic distribution of sedimentary climate indicators (e.g., coals and evaporites) also indicates hot and arid conditions for lower latitudes and much of Africa (Hallam, 1984, 1985). Incorporation of Late Jurassic phytogeographic data presents a similar picture, with a subtropical summer-wet climate near the equator and an arid desert zone poleward of ~10°S paleolatitude (Rees et al., 2000: Fig. 7C).

Recent GCM estimates of Late Jurassic surface temperature in Central Africa range from approximately 28 °C in austral winter (JJA) (Rees et al., 2000, Fig. 9B) to more than 40 °C in austral summer (DJF) (Sellwood and Valdes, 2006: Fig. 3A, 2008: Fig. 3A). The range of summer paleotemperatures estimated by these GCM studies is 28 °C to 44 °C, while the range of estimated winter paleotemperatures is slightly lower, between 28 °C and 36 °C (Rees et al., 2000: Fig. 9A–B; Sellwood and Valdes, 2006: Fig. 3A–B, 2008: Fig. 3A–B). Measurements at modern, low latitude soil-forming localities indicate that average annual soil temperatures are higher than mean annual air temperatures by approximately 5 °C (Passey et al., 2010). The range of maximum paleotemperature estimates produced here from isotopic analysis of clay minerals (25 °C to 40 °C) compares favorably with the results of GCM simulations, suggesting mean surface air temperatures between 20 °C and 35 °C. The overall results from geologic indicators and chemical proxies of paleoclimate are consistent with GCM results and suggest that Late Jurassic GCMs are able to predict paleoclimate accurately for tectonic and paleogeographic scenarios that are vastly different from modern.

6. Conclusions

Paleopedology and geochemical analysis demonstrate that hot and arid climate conditions prevailed in the deep interior of Gondwana during deposition of the Stanleyville Group. The presence of analcime and palygorskite is interpreted as evidence of hot and dry, saline lacustrine settings. Abundant vertic features throughout the Stanleyville section of the Samba core indicate that what little precipitation occurred within the continental interior was distributed seasonally. Lower soil CO_2 production estimates for the Stanleyville Group relative to the Morrison Formation are consistent with arid conditions in the Congo Basin inferred from paleosol morphology and matrix mineralogy. Oxygen and hydrogen isotope analysis of the fine clay fraction of paleosol matrix

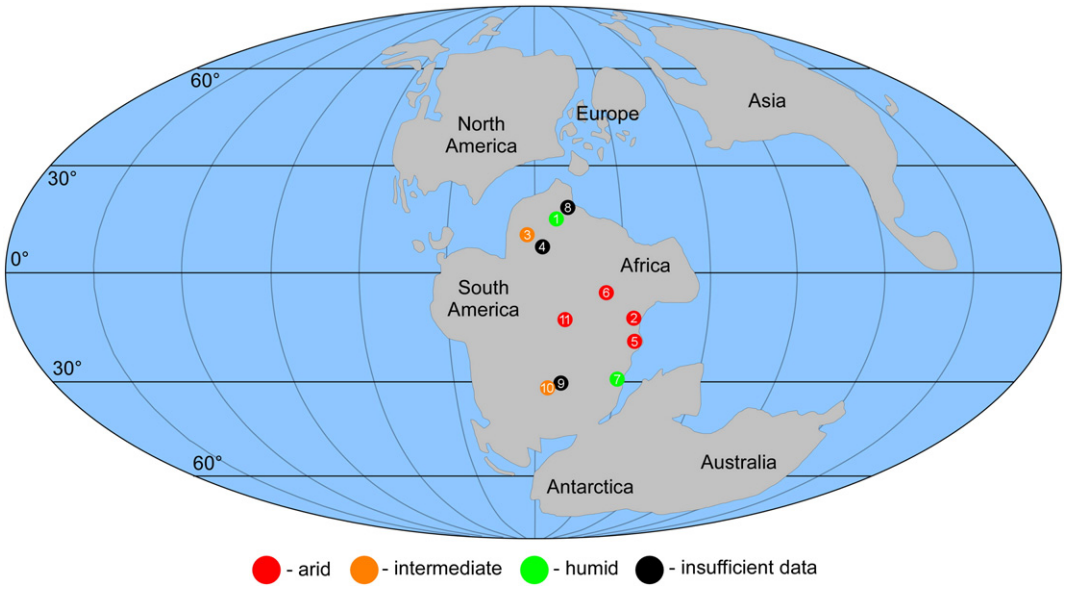

Fig. 10. Distribution of Upper Jurassic continental deposits in Africa. Numbers correspond to localities in Table 6. Dot colors correspond to paleoclimatic conditions inferred from sedimentological and paleobotanical evidence. Red = arid (precipitation ≪ evapotranspiration), green = humid (precipitation ≫ evapotranspiration), orange = intermediate (precipitation ≈ evapotranspiration), black = insufficient data to provide paleoenvironmental interpretation. Sites between 5°S and 20°S are characterized by arid paleoclimate with only a small amount of seasonal rainfall. North and south of this arid belt, more humid conditions prevail. Paleogeographic reconstruction modified from Smith et al. (1994).

samples provides soil temperature estimates between 25 °C and 40 °C, which are in accord with surface temperature estimates produced in GCM simulations for the Late Jurassic. Evidence from other Upper Jurassic, African continental localities between 5°S and 20°S paleolatitude suggest hot, arid climatic conditions similar to those reconstructed here for the Stanleyville Group. Some areas that developed closer to the coast retain evidence of more humid conditions, with higher weathering rates and enough precipitation to support growth of large woody plants.

Acknowledgments

We thank Luc Tack and Daniel Baudet of the Royal Museum for Central Africa for assistance with sampling the Samba core. Dale Winkler and Luc Tack provided helpful comments on an earlier version of this manuscript. This paper was also improved by critical comments from Nathan Sheldon, an anonymous reviewer, and editor Finn Surlyk. We are also indebted to Ian Richards of the Stable Isotope Laboratory at SMU who conducted the extraction of O_2 from phyllosilicate samples. Funding for this research was provided by the Roy M. Huffington Department of Earth Sciences and Institute for the Study of Earth and Man at SMU, as well as the Roy M. Huffington Graduate Fellowship awarded to TSM and NSF EAR-0617250 awarded to NJT.

References

Aberhan, M., Bussert, R., Heinrich, W.-D., Schrank, E., Schultka, S., Sames, B., Kriwet, J., Kapilima, S., 2002. Palaeoecology and depositional environments of the Tendaguru Beds (Late Jurassic to Early Cretaceous, Tanzania). Mitteilungen aus dem Museum für Naturkunde Berlin, Geowissenschaftliche Reihe 5, 19–44.

Ait-Kaci Ahmed, A., Lingham-Soliar, T., Broderick, T.J., 2004. Giant sauropod tracks from the Middle–Late Jurassic of Zimbabwe in close association with theropod tracks. Lethaia 37, 467–470.

Alessandrello, A., Teruzzi, G., 1989. New outcrops with dinosaurs trackways in the Cretaceous of the Agadez region, (eastern Niger). Atti della Società Italiana di Scienze Naturali e del Museo Civico di Storia Naturale di Milano 130 (12), 177–188.

Anderson, P.E., Benton, M.J., Trueman, C.N., Paterson, B.A., Cuny, G., 2007. Palaeoenvironments of vertebrates on the southern shore of Tethys: the nonmarine Early Cretaceous of Tunisia. Palaeogeography, Palaeoclimatology, Palaeoecology 243, 118–131.

Angelucci, A., Barbieri, F., Maxamed, C.M., Caynab, F.C., Franco, F., Carush, M.C., Piccoli, G., 1983. The Jurassic stratigraphic series in Gedo and Bay regions (southwestern Somalia). Memorie di Scienze Geologiche, Padova 36, 73–94.

Arkell, W.J., 1956. Jurassic Geology of the World. Hafner Publishing Company Inc., New York.

Arratia, G., Kriwet, J., Heinrich, W.-D., 2002. Selachians and actinopterygians from the Upper Jurassic of Tendaguru, Tanzania. Mitteilungen aus dem Museum für Naturkunde Berlin, Geowissenschaftliche Reihe 5, 207–230.

Assefa, G., 1991. Lithostratigraphy and environment of deposition of the Late Jurassic–Early Cretaceous sequence of the central part of Northwestern Plateau, Ethiopia. Neues Jahrbuch für Geologie und Paläontologie, Abhandlungen 182 (3), 255–284.

Awad, M.Z., Schrank, E., 1993. Palaeoecology of Late Jurassic to mid-Cretaceous of the central and western Sudan. In: Thorweihe, U., Schandelmeier, H. (Eds.), Geoscientific Research in Northeast Africa: Proceedings of the International Conference on Geoscientific Research in Northeast Africa, Berlin, Germany, 17–19 June 1993. A.A. Balkema, Rotterdam, pp. 369–374.

Bamford, M.K., Roberts, E.M., Sissoko, F., Bouaré, M.L., O'Leary, M.A., 2002. An extensive deposit of fossil conifer wood from the Mesozoic of Mali, southern Sahara. Palaeogeography, Palaeoclimatology, Palaeoecology 186, 115–126.

Benison, K.C., Goldstein, R.H., 1999. Permian paleoclimate data from fluid inclusions in halite. Chemical Geology 154, 113–132.

Benton, M.J., Bouaziz, S., Buffetaut, E., Martill, D.M., Ouaja, M., Soussi, M., Trueman, C., 2000. Dinosaurs and other fossil vertebrates from fluvial deposits in the Lower Cretaceous of southern Tunisia. Palaeogeography, Palaeoclimatology, Palaeoecology 157, 227–246.

Berner, R.A., 2006a. GEOCARBSULF: a combined model for Phanerozoic atmospheric O_2 and CO_2. Geochimica et Cosmochimica Acta 70, 5653–5664.

Berner, R.A., 2006b. Inclusion of the weathering of volcanic rocks in the GEOCARBSULF model. American Journal of Science 306, 295–302.

Berner, R.A., 2008. Addendum to "Inclusion of the Weathering of Volcanic Rocks in the GEOCARBSULF Model" (R. A. Berner, 2006, V. 306, P. 295–302). American Journal of Science 308, 100–103.

Berner, R.A., Kothavala, Z., 2001. GEOCARB III: a revised model of atmospheric CO_2 over Phanerozoic time. American Journal of Science 301, 182–204.

Birkeland, P.W., 1999. Soils and Geomorphology. Oxford University Press, New York.

Bond, G., Bromley, K., 1970. Sediments with the remains of dinosaurs near Gokwe, Rhodesia. Palaeogeography, Palaeoclimatology, Palaeoecology 8 (4), 313–327.

Bose, M.-N., 1974. A palynological reconnaissance of the Mesozoic sediments of Zaïre. Bulletin des Séances de Académie Royale des Sciences d'Outre-Mer 1974 (4), 618–628.

Boutton, T.W., 1991. Stable carbon isotope ratios of natural materials: I. Sample preparation and mass spectrometric analysis. In: Coleman, D.C., Fry, B. (Eds.), Carbon Isotope Techniques. Academic Press, Inc., New York, pp. 155–171.

Bradford, J.B., Lauenroth, W.K., Burke, I.C., Paruelo, J.M., 2006. The influence of climate, soils, weather, and land use on primary production and biomass seasonality in the US Great Plains. Ecosystems 9, 934–950.

Brooke, G.A., Gilbert, P.M., Ward, B.B., 1983. A world model of soil carbon dioxide. Earth Surface Processes and Landforms 8, 79–88.

Budyko, M.I., Ronov, A.B., Yanshin, A.L., 1985. Changes in the chemical composition of the atmosphere during the Phanerozoic. International Geology Review 27, 423–433.

Bumby, A.J., Guiraud, R., 2005. The geodynamic setting of the Phanerozoic basins of Africa. Journal of African Earth Sciences 43, 1–12.

Bussert, R., Heinrich, W.-D., Aberhan, M., 2009. The Tendaguru Formation (Late Jurassic to Early Cretaceous, southern Tanzania): definition, palaeoenvironments, and sequence stratigraphy. Fossil Record 12 (2), 141–174.

Busson, G., Cornée, A., 1991. The Sahara from the Middle Jurassic to the Middle Cretaceous: data on environments and climates based on outcrops in the Algerian Sahara. Journal of African Earth Sciences 12 (1/2), 85–105.

Buyanovsky, G.A., Wagner, G.H., 1983. Annual cycles of carbon dioxide level in soil air. Soil Science Society of America Journal 47, 1139–1145.

Cahen, L., 1983. Le Groupe de Stanleyville (Jurassique supérieur et Wealdien de l'intérieur de la République de Zaïre). Révision des connaissances. Rapport annuel du Department de geologie et de mineralogie du Musee royal de l'Afrique centrale 1981–82, 73–91.

Cahen, L., Lepersonne, J., 1955. Les formations Mésozoiques de l'intérieur du Congo. Resumé des connaissances et relations avec les régions limitrophes. Réunion de Nairobi: compte rendu et communications, pp. 221–228.

Cahen, L., Ferrand, J.J., Haarsma, M.J.F., Lepersonne, J., Verbeek, T., 1959. Description du Sondage de Samba. Annales du Musée royal du Congo Belge, Tervuren (Belgique). Série in-8°, Sciences géologiques 29, 1–210.

Callen, R.A., 1984. Clays of the palygorskite–sepiolite group: depositional environment, age and distribution. In: Singer, A., Galan, E. (Eds.), Palygorskite–Sepiolite: Occurrences, Genesis and Uses. : Developments in Sedimentology, 37. Elsevier, New York, pp. 1–37.

Capuano, R.M., 1992. The temperature dependence of hydrogen isotope fractionation between clay minerals and water: evidence from a geopressured system. Geochimica et Cosmochimica Acta 56 (6), 2547–2554.

Cerling, T.E., 1991. Carbon dioxide in the atmosphere: evidence from Cenozoic and Mesozoic paleosols. American Journal of Science 291, 377–400.

Cerling, T.E., Quade, J., 1993. Stable carbon and oxygen isotopes in soil carbonates. Climate Change in Continental Isotopic Records. Geophysical Monograph 78, 217–231.

Chorowicz, J., Le Fournier, J., Mvumbi, M.M., 1990. La Cuvette Centrale du Zaïre: un bassin initié au Protérozoïque supérieur. Contribution de l'analyse du réseau hydrographique. Comptes rendus de l'Académie des Sciences Paris. Série II 311, 349–356.

Churkina, G., Running, S.W., 1998. Contrasting climatic controls on the estimated productivity of global terrestrial biomes. Ecosystems 1, 206–215.

Clemens, W.A., Goodwin, M.B., Hutchison, J.H., Schaff, C.R., Wood, C.B., Colbert, M.W., 2007. First record of a Jurassic mammal (?"Peramura") from Ethiopia. Acta Palaeontologica Polonica 52 (3), 433–439.

Colin, J.P., 1994. Mesozoic–Cenozoic lacustrine sediments of the Zaïre Interior Basin. Global Geological Record of Lake Basins 4, 31–36.

Cooper, M.R., 1988. A new bivalve from the Late Jurassic of Zimbabwe. South African Journal of Geology 91 (3), 321–325.

Coulombe, C.E., Dixon, J.B., Wilding, L.P., 1996. Mineralogy and chemistry of Vertisols. In: Ahmad, N., Mermut, A. (Eds.), Vertisols and Technologies for Their Management. : Developments in Soil Science, 24. Elsevier, New York, pp. 115–200.

Cox, L.R., 1953. Lamellibranchs from the Lualaba beds of the Belgian Congo. Revue de Zoologie et de Botanique Africaines 47, 99–107.

Cox, L.R., 1960. Further Mollusca from the Lualaba beds of the Belgian Congo. Annales de Musée royal de l'Afrique centrale, Tervuren (Belgique). Série in 8°, Sciences géologiques 37, 1–15.

Crosby, A.G., Fishwick, S., White, N., 2010. Structure and evolution of the intracratonic Congo Basin. Geochemistry, Geophysics, Geosystems 11 (6), 1–20.

Curtis, C.D., 1990. Aspects of climatic influence on the clay mineralogy and geochemistry of soils, palaeosols and clastic sedimentary rocks. Journal of the Geological Society of London 147, 351–357.

Daly, M.C., Lawrence, S.R., Diemu-Tshiband, K., Matouana, B., 1992. Tectonic evolution of the Cuvette Centrale, Zaire. Journal of the Geological Society of London 149 (4), 539–546.

Dasog, G.S., Acton, D.F., Mermut, A.R., De Jong, E., 1988. Shrink–swell potential and cracking in clay soils of Saskatchewan. Canadian Journal of Soil Science 68, 251–260.

Defrétin-Lefranc, S., 1967. Étude sur les phyllopodes du bassin du Congo. Annales de Musée royal de l'Afrique centrale, Tervuren (Belgique). Série in 8°, Sciences géologiques 56, 1–122.

Delgado, A., Reyes, E., 1996. Oxygen and hydrogen isotope compositions in clay minerals: a potential single-mineral geothermometer. Geochimica et Cosmochimica Acta 60 (21), 4285–4289.

Do Campo, M., del Papa, C., Jiménez-Millán, J., Nieto, F., 2007. Clay mineral assemblages and analcime formation in a Palaeogene fluvial-lacustrine sequence (Maíz Gordo Formation Palaeogen) from northwestern Argentina. Sedimentary Geology 201, 56–74.

Dudal, R., Eswaran, H., 1988. Distribution, properties and classification of Vertisols. In: Wilding, L.P., Puentes, R. (Eds.), Vertisols: Their Distribution, Properties, Classification and Management. Texas A&M University Printing Center, College Station, TX, pp. 1–22.
Edwards, N.T., 1975. Effects of temperature and moisture on carbon dioxide evolution in a mixed deciduous forest floor. Soil Science Society of America Journal 39, 361–365.
Egoroff, A., Lombard, A.L., 1962. Présence des couches de Stanleyville dans le sous-sol de Léopoldville, République du Congo—Note préliminaire. Annales de la Société Géologique de Belgique 85 (1–4), 103–109.
Ekart, D.D., Cerling, T.E., Montañez, I.P., Tabor, N.J., 1999. A 400 million year carbon isotope record of pedogenic carbonate: implications for paleoatmospheric carbon dioxide. American Journal of Science 299, 805–827.
English, P.M., 2001. Formation of analcime and moganite at Lake Lewis, central Australia: significance of groundwater evolution in diagenesis. Sedimentary Geology 143, 219–244.
Foster, J.R., 2003. Paleoecological analysis of the vertebrate fauna of the Morrison Formation (Upper Jurassic), Rocky Mountain Region, U.S.A. New Mexico Museum of Natural History and Science Bulletin 23, 1–95.
Garrett, H.E., Cox, G.S., 1973. Carbon dioxide evolution from the floor of an oak–hickory forest. Soil Science Society of America Journal 37, 641–644.
Gile, L.H., Peterson, F.F., Grossman, R.B., 1966. Morphological and genetic sequences of carbonate accumulation in desert soils. Soil Science 101 (5), 347–360.
Ginsburg, L., Lapparent, A.F., Loiret, B., Taquet, P., 1966. Empreintes de pas de Vertébrés tétrapodes dans les séries continentales à l'Ouest d'Agadès (République du Niger). Comptes rendus hebdomadaires des séances de l'Académie des sciences. D, Sciences naturelles 263 (1), 28–31.
Giresse, P., 2005. Mesozoic–Cenozoic history of the Congo Basin. Journal of African Earth Sciences 43, 301–315.
Golonka, J., Edrich, M.E., Ford, D.W., Pauken, R.J., Bocharova, N.Y., Scotese, C.R., 1996. Jurassic paleogeographic maps of the world. In: Morales, M. (Ed.), The Continental Jurassic: Museum of Northern Arizona Bulletin, 60, pp. 1–5. Flagstaff.
Goodwin, M.B., Clemens, W.A., Hutchison, J.H., Wood, C.B., Zavada, M.S., Kemp, A., Duffin, C.J., Schaff, C.R., 1999. Mesozoic continental vertebrates with associated palynostratigraphic dates from the northwestern Ethiopian plateau. Journal of Vertebrate Paleontology 19 (4), 728–741.
Grekoff, N., 1957. Ostracodes du bassin du Congo. I. Jurassique supérieur et Crétacé inférieur du nord du bassin. Annales de Musée royal de l'Afrique centrale, Tervuren (Belgique). Série in 8°, Sciences géologiques 19, 1–97.
Guiraud, R., Bosworth, W., Thierry, J., Delplanque, A., 2005. Phanerozoic geological evolution of Northern and Central Africa: an overview. Journal of African Earth Sciences 43, 83–143.
Hallam, A., 1984. Continental humid and arid zones during the Jurassic and Cretaceous. Palaeogeography, Palaeoclimatology, Palaeoecology 47, 195–223.
Hallam, A., 1985. A review of Mesozoic climates. Journal of the Geological Society of London 142 (3), 433–445.
Hallam, A., 2001. A review of the broad pattern of Jurassic sea-level changes and their possible causes in the light of current knowledge. Palaeogeography, Palaeoclimatology, Palaeoecology 167, 23–37.
Hartley, A., Flint, S., Turner, P., 1991. Analcime: a characteristic authigenic phase of Andean alluvium, northern Chile. Geological Journal 26, 189–202.
Hill, G., 1989. Distal alluvial fan sediments from the Upper Jurassic of Portugal: controls on their cyclicity and channel formation. Journal of the Geological Society of London 146 (3), 539–555.
Kadima, E., Delvaux, D., Sebagenzi, S.N., Tack, L., Kabeya, S.M., 2011a. Structure and geological history of the Congo Basin: an integrated interpretation of gravity, magnetic and reflection seismic data. Basin Research. doi:10.1111/j.1365-2117.2011.00500.x.
Kadima, E.K., Sebagenzi, S.M.N., Lucazeau, F., 2011b. A Proterozoic-rift origin for the structure and the evolution of the cratonic Congo basin. Earth and Planetary Science Letters 304, 240–250.
Khademi, H., Mermut, A.R., 1998. Source of palygorskite in gypsiferous Aridisols and associated sediments from central Iran. Clay Minerals 33, 561–578.
Kowallis, B.J., Christiansen, E.H., Deino, A.L., Peterson, F., Turner, C.E., Kunk, M.J., Obradovich, J.D., 1998. The age of the Morrison Formation. Modern Geology 22, 235–260.
Lawrence, S.R., Mvumbi, M.M., 1988. Zaire's Central basin: prospectivity outlook. Oil & Gas Journal 86 (38), 105–108.
Lepersonne, J., 1974. Carte géologique du Zaïre, Éschelle 1:2,000,000. Republique du Zaïre, Commissaritate d'Etat aux Mines, Service Géologique.
Lepersonne, J., 1977. Structure géologique du bassin du Zaïre. Académie royale de Belgique. Bulletin de la Classe des sciences 63, 941–965.
Leriche, M., 1911. Les poissons des couches du Lualaba (Congo Belge). Revue Zoologique Africaine 1, 190–197.
Lieth, H., 1975. Modeling the primary productivity of the world. In: Lieth, H., Wittaker, R.H. (Eds.), Primary Productivity of the Biosphere. Springer Verlag, New York, pp. 237–263.
López-Arbarello, A., Rauhut, O.W.M., Moser, K., 2008. Jurassic fishes of Gondwana. Revista de la Asociación Geológica Argentina 63 (4), 586–612.
Mack, G.H., James, W.C., 1994. Paleoclimate and the global distribution of paleosols. Journal of Geology 102, 360–366.
Mack, G.H., James, W.C., Monger, H.C., 1993. Classification of paleosols. Geological Society of America Bulletin 105, 129–136.
Marriott, S.B., Wright, V.P., 1993. Palaeosols as indicators of geomorphic stability in two Old Red Sandstone alluvial suites, South Wales. Journal of the Geological Society of London 150 (6), 1109–1120.
McCrea, J.M., 1950. On the isotopic chemistry of carbonates and a paleotemperature scale. Journal of Chemical Physics 18 (6), 849–857.
Melillo, J.M., McGuire, A.D., Kicklighter, D.W., Moore III, B., Vorosmarty, C.J., Schloss, A.L., 1993. Global climate change and terrestrial net primary production. Nature 363, 234–240.
Mora, C.I., Fastovsky, D.E., Driese, S.G., 1993. Geochemistry and stable isotopes of paleosols. University of Tennessee Studies in Geology 23, 1–65.
Nemani, R.R., Keeling, C.D., Hashimoto, H., Jolly, W.M., Piper, S.C., Tucker, C.J., Myneni, R.B., Running, S.W., 2003. Climate-driven increases in global terrestrial net primary production from 1982 to 1999. Science 300 (5625), 1560–1563.
Parrish, J.T., 1993. Climate of the supercontinent Pangea. Journal of Geology 101, 215–233.
Passey, B.H., Levin, N.E., Cerling, T.E., Brown, F.H., Eiler, J.M., 2010. High-temperature environments of human evolution in East Africa based on bond ordering in paleosol carbonates. Proceedings of the National Academy of Sciences 107 (25), 11245–11249.
Peterson, F., 1988. Stratigraphy and nomenclature of Middle and Upper Jurassic rocks, western Colorado Plateau, Utah and Arizona. U.S. Geological Survey Bulletin 1633-B, 1–43.
Quast, A., Hoefs, J., Paul, J., 2006. Pedogenic carbonates as a proxy for palaeo-CO_2 in the Palaeozoic atmosphere. Palaeogeography, Palaeoclimatology, Palaeoecology 242, 110–125.
Raath, M.A., McIntosh, J.S., 1987. Sauropod dinosaurs from the Central Zambezi Valley, Zimbabwe, and the age of the Kadzi Formation. South African Journal of Geology 90 (2), 107–119.
Rauhut, O.W.M., López-Arbarello, A., 2009. Considerations on the age of the Tiouaren Formation (Iullemmeden Basin, Niger, Africa): implications for Gondwanan Mesozoic terrestrial vertebrate faunas. Palaeogeography, Palaeoclimatology, Palaeoecology 271, 259–267.
Rees, P.M., Ziegler, A.M., Valdes, P.J., 2000. Jurassic phytogeography and climates: new data and model comparisons. In: Huber, B.T., Macleod, K.G., Wing, S.L. (Eds.), Warm Climates in Earth History. Cambridge University Press, Cambridge, pp. 297–318.
Romanek, C.S., Grossman, E.L., Morse, J.W., 1992. Carbon isotopic fractionation in synthetic aragonite and calcite: effects of temperature and precipitation rate. Geochimica et Cosmochimica Acta 56, 419–430.
Royer, D.L., 2006. CO_2-forced climate thresholds during the Phanerozoic. Geochimica et Cosmochimica Acta 70, 5665–5675.
Saint-Seine, P., 1955. Poissons fossiles de l'etage de Stanleyville (Congo belge): Premiere partie. La faune des argilites et schistes bitumineux. Annales de Musée royal de l'Afrique centrale, Tervuren (Belgique). Série in 8°, Sciences géologiques 14, 1–126.
Saint-Seine, P., Casier, E., 1962. Poissons fossiles des couches de Stanleyville (Congo): Deuxième partie. La faune marine des Calcaires de Songa. Annales de Musée royal de l'Afrique centrale, Tervuren (Belgique). Série in 8°, Sciences géologiques 44, 1–52.
Saint-Seine, P., Cahen, L., Lepersonne, J., 1952. L'âge de l'étage de Stanleyville (série du Lualaba) et ses conséquences pour la stratigraphie du Congo. Bulletin de la Société Belge de Géologie de Paléontologie et d'Hydrologie 61, 198–207.
Sames, B., 2008. Application of Ostracoda and Charophyta from the Late Jurassic to Early Cretaceous Tendaguru formation at Tendaguru, Tanzania (East Africa)—biostratigraphy, palaeobiogeography and palaeoecology. Palaeogeography, Palaeoclimatology, Palaeoecology 264, 213–229.
Savin, S.M., Epstein, S., 1970. The oxygen and hydrogen isotope geochemistry of clay minerals. Geochimica et Cosmochimica Acta 34, 25–42.
Savin, S.M., Hsieh, J.C.C., 1998. The hydrogen and oxygen isotope geochemistry of pedogenic clay minerals: principles and theoretical background. Geoderma 82, 227–253.
Schmidt, D., Werner, C., 1998. Early Cretaceous coastal plain sediments of the Mugher Mudstone Formation, Abay River Basin, Ethiopia. Zentralblatt für Geologie und Paläontologie, Teil I 1997 (1/2), 293–309.
Schudack, M.E., Turner, C.E., Peterson, F., 1998. Biostratigraphy, paleoecology and biogeography of charophytes and ostracodes from the Upper Jurassic Morrison Formation, Western Interior, USA. Modern Geology 22, 379–414.
Scotese, C.R., 2002. PALEOMAP Software: Point Tracker. PALEOMAP Project, Arlington, TX.
Sellwood, B.W., Price, G.D., 1993. Sedimentary facies as indicators of Mesozoic palaeoclimate. Philosophical Transactions of the Royal Society of London, Series B 341, 225–233.
Sellwood, B.W., Valdes, P.J., 2006. Mesozoic climates: general circulation models and the rock record. Sedimentary Geology 190, 269–287.
Sellwood, B.W., Valdes, P.J., 2008. Jurassic climates. Proceedings of the Geologists' Association 119 (1), 5–17.
Sheldon, N.D., Tabor, N.J., 2009. Quantitative paleoenvironmental and paleoclimatic reconstruction using paleosols. Earth-Science Reviews 95, 1–52.
Singer, A., 1984. Pedogenic palygorskite in the arid environment. In: Singer, A., Galan, E. (Eds.), Palygorskite–Sepiolite: Occurrences, Genesis and Uses. : Developments in Sedimentology, 37. Elsevier, New York, pp. 169–176.
Smith, A.G., Smith, D.G., Funnell, B.M., 1994. Atlas of Mesozoic and Cenozoic Coastlines. Cambridge University Press, Cambridge. 99 pp.
Stough, J.B., 1965. Paleozoic and Mesozoic palynomorphs from the Republic of Congo. Esso, Stratigraphic and Structural Geology Division, Unpublished report, 4 pp.
Tabor, N.J., Montañez, I.P., Southard, R.J., 2002. Paleoenvironmental reconstruction from chemical and isotopic compositions of Permo-Pennsylvanian pedogenic minerals. Geochimica et Cosmochimica Acta 66 (17), 3093–3107.
Tabor, N.J., Yapp, C.J., Montanez, I.P., 2004. Goethite, calcite, and organic matter from Permian and Triassic soils: carbon isotopes and CO_2 concentrations. Geochimica et Cosmochimica Acta 68 (7), 1503–1517.

Turner, C.E., Peterson, F., 2004. Reconstruction of the Upper Jurassic Morrison Formation extinct ecosystem—a synthesis. Sedimentary Geology 167, 309–355.
Uchupi, E., 1988. The Mesozoic–Cenozoic geologic evolution of Iberia, a tectonic link between Africa and Europe. Revista de la Sociedad Geológica de España 1 (3–4), 257–294.
Valdes, P.J., Sellwood, B.W., 1992. A palaeoclimate model for the Kimmeridgian. Palaeogeography, Palaeoclimatology, Palaeoecology 95, 47–72.
Vanderstappen, R., Verbeek, T., 1964. Analcime et mineraux argileux. Annales de Musée royal de l'Afrique centrale, Tervuren (Belgique). Série in 8°, Sciences géologiques 47, 1–88.
Veatch, A.C., 1935. Evolution of the Congo Basin. Geological Society of America Memoir 3, 1–183.
Veizer, J., Ala, D., Azmy, K., Bruckschen, P., Buhl, D., Bruhn, F., Carden, G.A.F., Diener, A., Ebneth, S., Godderis, Y., Jasper, T., Korte, C., Pawellek, F., Podlaha, O.G., Strauss, H., 1999. $^{87}Sr/^{86}Sr$, $\delta^{13}C$ and $\delta^{18}O$ evolution of Phanerozoic seawater. Chemical Geology 161, 59–88.
Vernet, J.-P., 1961. Concerning the association montmorillonite–analcime in the series of Stanleyville, Congo. Journal of Sedimentary Petrology 31 (2), 293–295.
Vitali, F., Longstaffe, F.J., McCarthy, P.J., 2002. Stable isotopic investigation of clay minerals and pedogenesis in an interfluve paleosol from the Cenomanian Dunvegan Formation, N.E. British Columbia, Canada. Chemical Geology 192, 269–287.
Wilding, L.P., Tessier, D., 1988. Genesis of Vertisols: shrink–swell phenomena. In: Wilding, L.P., Puentes, R. (Eds.), Vertisols: Their Distribution, Properties, Classification and Management. Texas A&M University Printing Center, College Station, TX, pp. 55–81.
Witkamp, M., 1966. Rates of carbon dioxide evolution from the forest floor. Ecology 47 (3), 492–494.
Yanbin, S., Gallego, O.F., Martínez, S., 2004. The chonchostracan subgenus *Orthestheria* (*Migransia*) from the Tacuarembó Formation (Late Jurassic–?Early Cretaceous, Uruguay) with notes on its geological age. Journal of South American Earth Sciences 16, 615–622.
Zein el Abedine, A., Robinson, G.H., 1971. A study on cracking in some Vertisols of the Sudan. Geoderma 5, 229–241.